THE UNIVERSITY OF CHICAGO

TRANSCRIPTIONAL PROFILING OF PLANT RESPONSE TO PHYTOSULFOKINE PEPTIDE REVEALS NOVEL SIGNALING OUTPUTS

A DISSERTATION SUBMITTED TO

THE FACULTY OF THE DIVISION OF THE BIOLOGICAL SCIENCES

AND THE PRITZKER SCHOOL OF MEDICINE

IN CANDIDACY FOR THE DEGREE OF

DOCTOR OF PHILOSOPHY

GRADUATE PROGRAM IN BIOCHEMISTRY AND MOLECULAR BIOPHYSICS

BY

DIAN LIU

CHICAGO, ILLINOIS

JUNE 2024

TABLE OF CONTENTS

LIST OF FIGURES

LIST OF TABLES

ACKNOWLEDGMENTS

It has been a long and winding road towards the PhD.

Thanks to my parents for their lifetime unconditional love.

Thanks to my advisor, Dr. Jean Greenberg. Her guidance, patience and understanding are the reasons I could make it through.

Thanks to my committee members, Dr. David Kovar, Dr. Demet Araç-Özkan, Dr. Alexander Ruthenburg. Their advice, support and dedication are vital for my academic journey.

Thanks to the Greenberg lab, BMB program and BSD division for providing the valuable training opportunity.

Thanks to all the people I have met and spent time with during these years.

Along the way, there were as many hard nights as there were happy days.

One day, the graduation came close, I began to realize that these years are my finest and brightest age. Part of me will forever remain in Hyde Park, Chicago.

ABSTRACT

Phytosulfokine (PSK) is a plant growth-promoting peptide hormone that is perceived by its cell surface receptors PSKR1 and PSKR2 in Arabidopsis. Plants lacking the PSK receptors show phenotypes consistent with PSK signaling repressing some plant defenses. However, the degree to which such repression is an indirect effect of receptor mutations or directly linked to the presence and effects of PSK was unclear.

To fill this gap in knowledge, comprehensive transcriptional profiling of Arabidopsis treated with PSK was performed and PSK treatment's effects on plant defense readouts were monitored. WRKY transcription factors emerged as key regulators of PSK-responsive genes, sharing commonality with pathogen-associated molecular pattern (PAMP) responses, but exhibiting opposite regulatory directions. These PSK-induced transcriptional changes were accompanied by biochemical and physiological changes that reduced PAMP responses, notably Mitogen-Activated Protein Kinase phosphorylation (previously implicated in WRKY activation) and the cell wall modification of callose deposition. My study indicates stronger suppression of defense genes than induction of growth-related genes and supports a role for PSK signaling in mediating a trade-off between plant growth and defense.

1 CHRACTERIZATION OF PSK SIGNALING PATHWAY RELATED MUTANTS AND VALIDATION OF PSK PEPTIDE ACTIVITY

1.1 Overview of PSK signaling

Like animals, plants also have signaling systems that control their development and help them adapt to changing environments. In many cases, adaptation is mediated by non-proteinaceous phytohormones like auxins and gibberellins [1, 2]. However, many secreted peptides also play important roles in plant signaling via cell surface receptors [3-5].

Phytosulfokine (PSK) is a disulfated pentapeptide Tyr(SO_3H)-Ile-Tyr(SO_3H)-Thr-Gln [6]. It is synthesized from prepropeptides encoded by five precursor genes (PSK1-5) [7,8]. The prepropeptides are sulfated by tyrosylprotein sulfotransferase (TPST), which is a membrane-bound enzyme localized in the *trans*-Golgi network and encoded by a single gene in Arabidopsis [9]. This enzyme also sulfates other plant peptides including Plant Peptide Containing Sulfated Tyrosine (PSY) and Root Growth Meristem Factor [10]. Sulfated PSK precursors subsequently undergo proteolytic cleavage in apoplast and become active pentapeptides [10]. In Arabidopsis PSK is perceived by PSK receptors (PSKR1 and PSKR2) [11, 12], that localize to the plasma membrane [13]. PSK receptors are receptor-like kinases with an extracellular domain, a single transmembrane helix and an intracellular kinase domain [14]. So far, no functional differences were reported for the two receptors, but PSKR1 is more well-studied [15]. The extracellular domain of PSKR1 consists of a leucine-rich repeat (LRR) region with 21 LRRs, and a 36-amino acid island domain intercepts LRRs 17 and 18 [14]. A 15-amino acid fragment of the island domain (Glu503-Lys517) was identified as a ligand binding site [16] and PSK binding causes allosteric

activation of PSKR1 [17]. PSKR1 is a calmodulin-binding protein that can associate with Ca^{2+} *in planta* [18]. Ca^{2+} regulates both the kinase and guanylate cyclase activities of PSKR1 *in vitro* [19]. To date, the kinase substrates and cGMP-regulated proteins, transcription factors and gene targets have not been identified [20] (Figure 1).

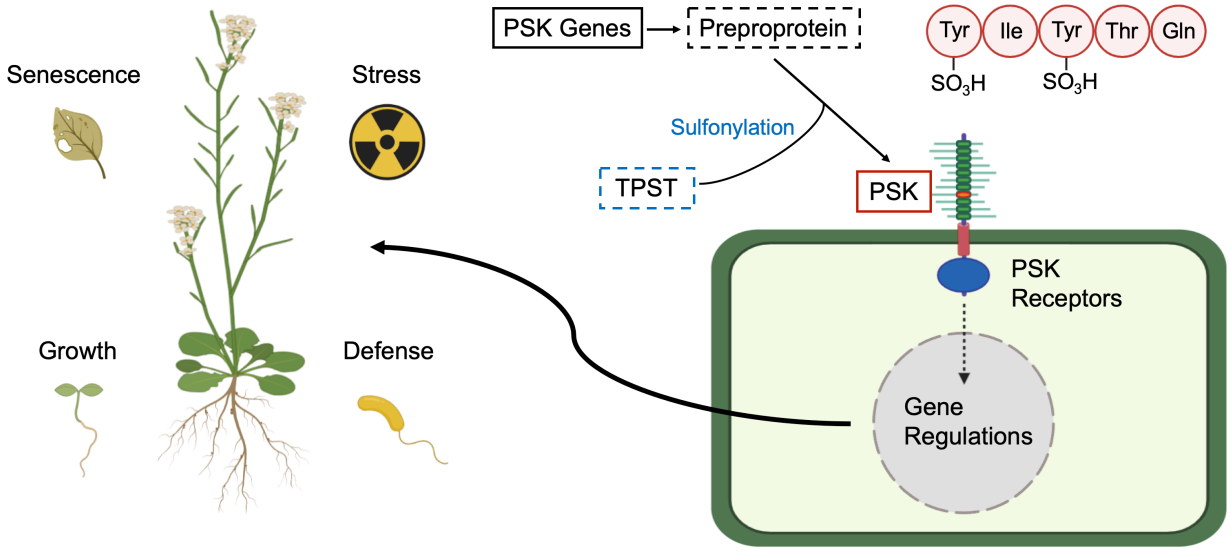

Figure 1. PSK signaling overview. PSK is perceived by its cell surface receptors PSKRs and leads to gene regulation changes that associated with growth, defense, stress and senescence. TPST-mediated sulfonylation is critical to PSK physiological activity.

1.2 Current knowledge about PSK function

Previous studies have illustrated PSK's role in promoting root elongation and leaf growth via cell division and cell growth promotion effects [11, 21, 22]. PSK signaling has been inferred to play an important part in regulating plant defense response. PSKR1 loss-of-function mutant *pskr1* displays enhanced pathogen-associated molecular pattern (PAMP) responses after infection with *Pseudomonas syringae* pv. tomato DC3000, suggesting PSK signaling attenuates immune responses induced by this bacterial pathogen [23]. However, the *pskr1* mutant is also more

susceptible to the necrotrophic fungal infection with *Alternaria brassicicola*, indicating PSK signaling increases immune response induced by a fungal pathogen [23]. A later study demonstrated that the *pskr1* mutant shows autoimmunity in response to growth-promoting *P. fluorescens*. Transcriptional profiling supported a role for PSKR1 in suppressing defenses regulated by the signal molecule salicylic acid [24]. Nonetheless, the transcriptional readouts of PSK's effects on plant are still lacking, and the relationship of transcriptomic changes and plant defense responses have yet to be well characterized.

1.3 Characterization of PSK signaling pathway-related mutants

I genotyped plant mutants related to the PSK signaling pathway from various sources and obtained homozygous *tpst*, *pskr1*, *pskr2* single mutants and *pskr1 pskr2* double mutant to study PSK signaling pathway. *tpst* plants cannot produce native active PSK peptide due to the lack of sulfonylation mediated by TPST enzyme. *pskr1* and *pskr2* single mutant plants and *pskr1 pskr2* double mutant plants lack the receptors of PSK peptide. I also obtained wild-type (WT, Col-0) plants transformed by *35S::PSKR1-GFP* and confirmed 35S::PSKR1-GFP localization at the plasma membrane using confocal microcopy (Figure 2). Under the constitutive CaMV 35S promoter, *35S::PSKR1-GFP* transformed plants have constitutive expression of PSKR1-GFP in addition to their native PSKR1, thus they likely have elevated PSKR1 accumulation.

I grew the plant mutants on plates vertically and measured their root lengths (Figure 2). Compared to WT, *tpst* plants had significantly shorter roots, while *35S::PSKR1-GFP*-transformed plants had longer primary roots, more lateral roots and larger shoots (Figure 2, 3). Single receptor mutant plants of *pskr1* and *pskr2* had root lengths similar to WT plants. However, the receptor double mutant plants *pskr1 pskr2* had shorter roots than WT plants (Figure 2, 3). This indicates

PSK signaling positively contributes to plant root growth [11, 21, 22]. Moreover, *tpst* plants were smaller than WT after being transferred to soil, indicating TPST's important role in promoting plant growth and enhancing plant biomass during the whole life cycle of plant (Figure 2).

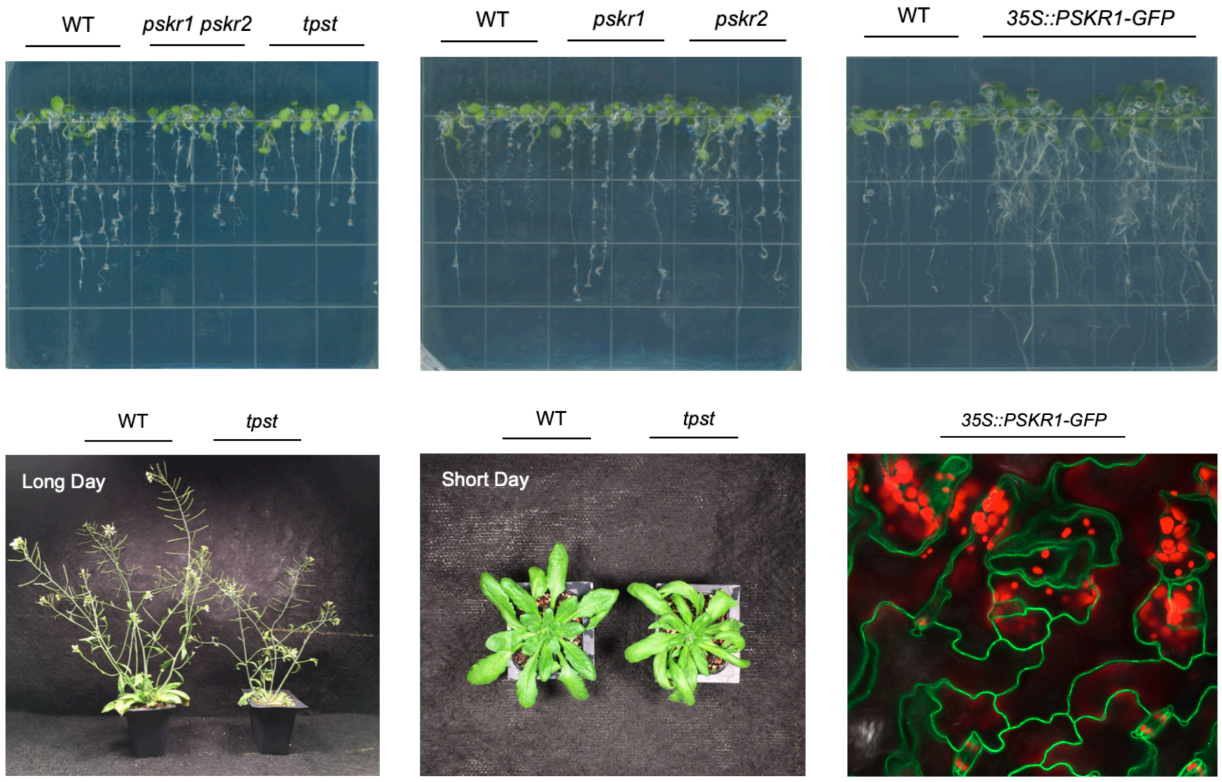

Figure 2. The phenotype of PSK signaling pathway-related plant lines. Plants were grown on plates with 1/2 Murashige and Skoog (MS) medium supplement with 1% sucrose vertically in long day condition after winterization for 3 days at 4 °C. The images of plants on plates were taken on the 9th day after winterization. 14 days after winterization, plants were transferred to soil and placed in long day condition and short day condition respectively until finishing their life cycles. The images of plants in soil were taken on the 38th day after winterization. The localization of PSKR1-GFP at the plasma membranes was confirmed by confocal microscope. Green color represents the PSKR1-GFP signal and red color represents the autofluorescence of chloroplast.

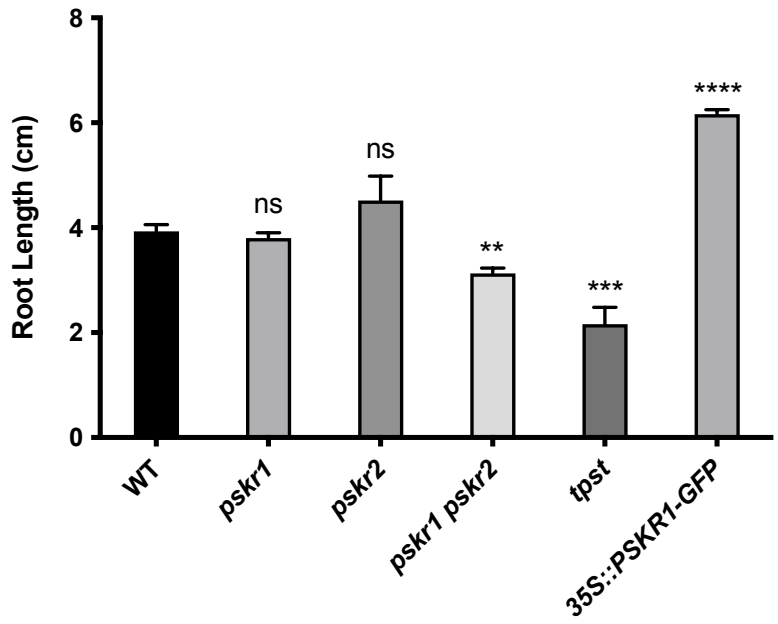

Figure 3. Root lengths of PSK signaling pathway-related plant lines on the 9th day after winterization. The root lengths of each plant line were quantified using the images of plate scans as shown in Figure 2 by Fiji. The root length of each plant line was compared to WT control. The root lengths were plotted as mean with SD; asterisks indicate significance under one-way ANOVA Fisher's test with p-value < 0.05, n = 5.

1.4 Validation of synthetic PSK activity in root growth promoting effect

In order to investigate the direct effects of PSK, I utilized *tpst* plants and treated them with synthetic PSK peptide to eliminate the effects of native active PSK produced by plants. Moreover, I included non-sulfated PSK (nsPSK) as a control to illustrate the peptide specificity and the importance of sulfonylation to PSK activity.

The activity of synthetic PSK and non-sulfated PSK (nsPSK) were tested by examining the root growth promotion effet of PSK. WT, *tpst* and *pskr1 pskr2* plants were grown on plates supplemented with PSK or nsPSK respectively under a gradient of concentrations. The root growth promotion effects were observed in *tpst* plants with PSK treatments but not with nsPSK treatments,

indicating the sulfonylation is critical to the activity of PSK (Figure 4). The PSK receptor double mutant *pskr1 pskr2* plants exhibited no root growth promotion effects from either PSK or nsPSK treatments, suggesting the specificity of PSK is dependent on its receptors (Figure 4). The root length of WT plants were only enhanced by > 10 nM PSK concentrations, whereas *tpst* roots responded to the low concentration of 10 nM PSK, showing *tpst* plants were more sensitive to PSK than WT plants that make native active PSK (Figure 4). Notably, nsPSK was able to promote root growth only at high concentrations in WT, *tpst* and *pskr1 pskr2* plants (Figure 4). This may occur due to nsPSK's weak binding activity to PSK receptors or nsPSK's indirect effects on root growth, such as a nutritional effect. Taken together, PSK's root growth promotion effect is associated with its sulfonylation and this effect is dependent on functional PSK receptors.

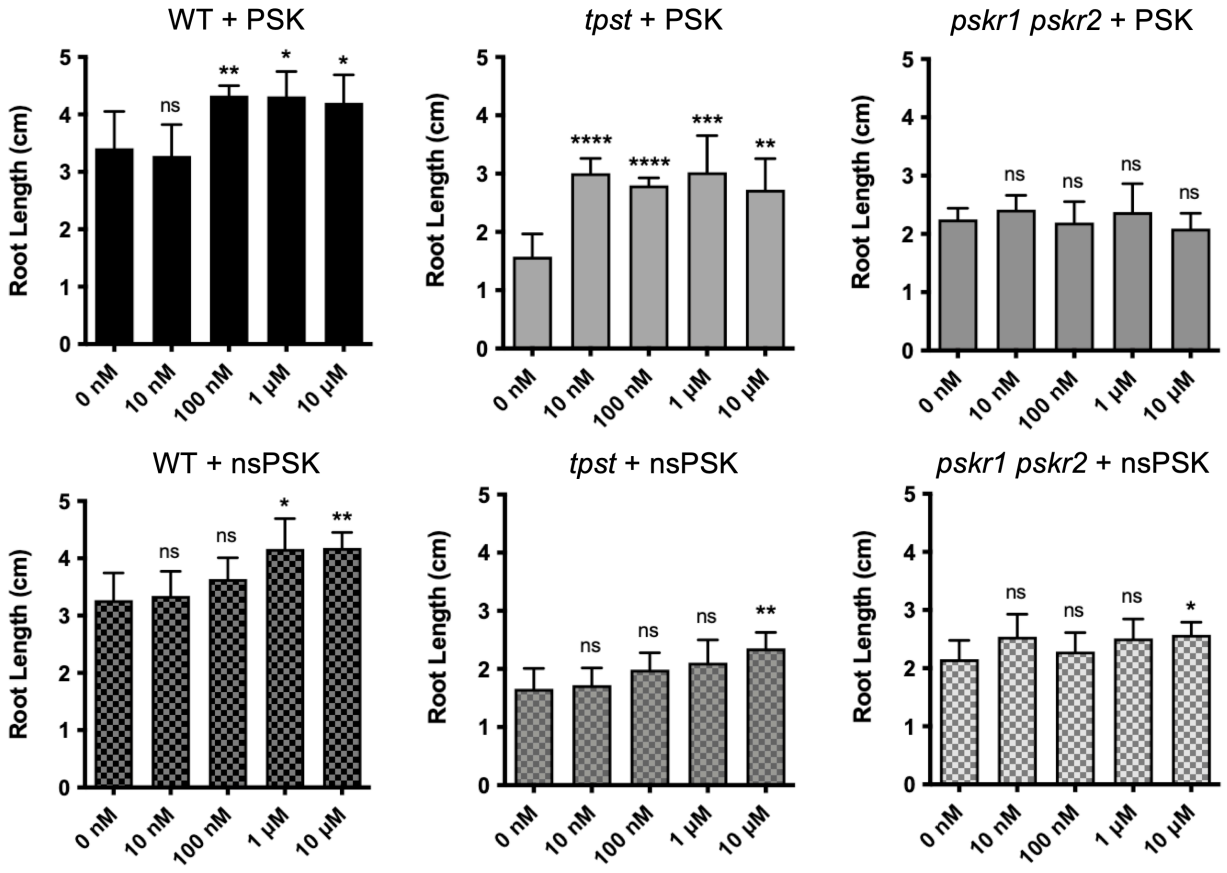

Figure 4. Root lengths of WT, *tpst*, *pskr1 pskr2* plants grown on plates supplemented with different concentrations of PSK and nsPSK. The images of plants grown on plates were taken on the 9th day after winterization and were subsequently used for root length quantification by Fiji. The root lengths of treated WT, *tpst* and *pskr1 pskr2* plants were compared to untreated control. The root lengths were plotted as mean with SD; asterisks indicate significance under one-way ANOVA Fisher's test with p-value < 0.05, n = 6.

1.5 The phenotype of plants grown in liquid medium is consistent with plants grown on plates

To enable precise control of the concentration and duration of PSK treatments, I utilized a hydroponic setting to have plants grown in 6-well cell culture dishes filled with 5 ml liquid 1/2 MS medium. The PSK treatments were conducted either by replacing the medium with new

medium containing desired concentrations of PSK and nsPSK, or by directly adding PSK and nsPSK to the medium to achieve the desired concentration.

The root length and shoot size phenotype of plants grown in liquid medium were consistent with results observed with plants grown on plates, with *tpst* plants displaying shorter root lengths and less shoot biomass, respectively, compared to WT plants (Figure 5, 6). 10 nM PSK was sufficient to promote the root length of *tpst* plants, but not *pskr1 pskr2* plants, while 10 nM nsPSK did not promote root growth in both cases (Figure 6).

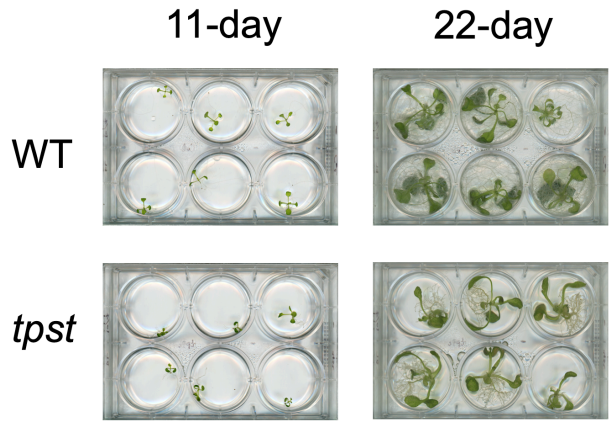

Figure 5. The phenotype of WT and *tpst* plants grown in liquid medium. The phenotypes that *tpst* plants displayed shorter root length and smaller shoot size compared to WT plants were consistent with the phenotypes seen in plants grown on agar plates or in soil.

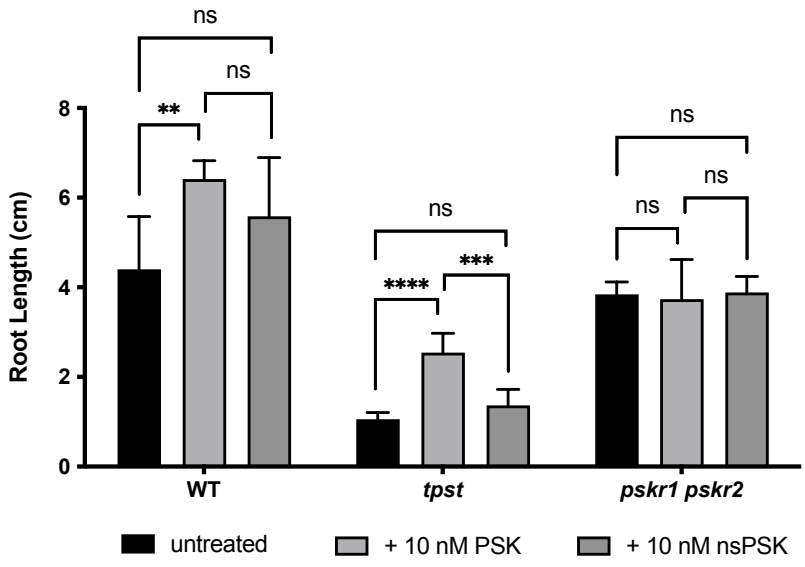

Figure 6. Root lengths of WT, *tpst*, *pskr1 pskr2* plants grown in liquid medium supplemented with 10 nM PSK and 10 nM nsPSK. The images of plants grown in liquid medium were taken on the 9th day after winterization and were subsequently used for root length quantification by Fiji. The root lengths of treated WT, *tpst* and *pskr1 pskr2* plants were compared to untreated control. The root lengths were plotted as mean with SD; asterisks indicate significance under one-way ANOVA Fisher's test with p-value < 0.05, n = 6.

1.6 PSK's root growth promotion effect is duration-dependent

In order to determine if PSK's root growth promotion effect is dependent on the duration of treatment, WT and *tpst* plants were grown in liquid medium supplemented with 10 nM PSK for different durations of treatments. At day 0, WT and *tpst* plants were grown in liquid medium supplemented with or without 10 nM PSK. At day 4, the medium were replaced by new medium supplemented with or without 10 nM PSK. This process exposed plants to 10 nM PSK for 0 days, 4 days, and 8 days respectively. The root length of *tpst* plants exposed to 10 nM PSK for 8 days were longer than *tpst* plants exposed to 10 nM for 4 days, and in both cases the root length were longer than *tpst* plants without PSK treatment (Figure 7). Therefore, PSK's root growth promotion

effect is dependent on the duration of PSK treatment, and longer exposure to PSK leads to a more significant enhancement.

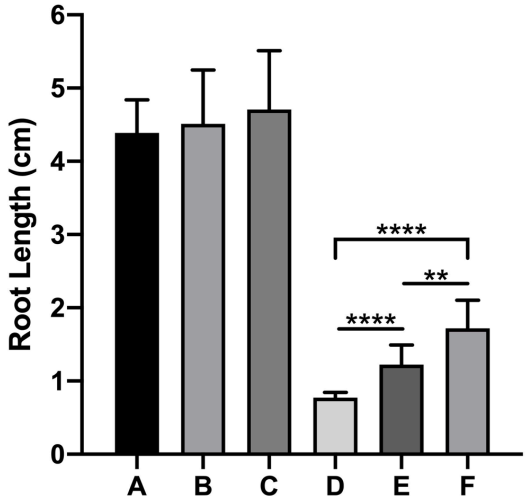

		Day 0	Day 4
A	Wild type	+0	+0
B	Wild type	+0	+10nM PSK
C	Wild type	+10nM PSK	+10nM PSK
D	tpst	+0	+0
E	tpst	+0	+10nM PSK
F	tpst	+10nM PSK	+10nM PSK

Figure 7. Root lengths of WT and *tpst* plants grown in liquid medium with different duration of PSK treatments. The images of plants grown in liquid medium were taken on the 8th day after winterization and were subsequently used for root length quantification by Fiji. The root lengths of PSK-treated WT and *tpst* plants were compared to untreated controls. The root lengths were plotted as mean with SD; asterisks indicate significance under one-way ANOVA Fisher's test with p-value < 0.05, n = 10.

2 TRANSCRIPTIONAL PROFILING OF PLANT RESPONSE TO PSK

2.1 RNA-seq experimental design

To eliminate endogenous PSK signaling, I utilized the *tpst* plants, which cannot produce native active sulfated PSK peptide, for transcriptional profiling. I did transcriptional profiling of *tpst* plants treated with synthetic PSK peptide using RNA-seq to capture gene expression readouts.

I grew *tpst* plants for 11 days in hydroponic conditions and treated plants with 10 nM PSK for 30 minutes, 2 hours and 5 hours to gain early responses to PSK; I also utilized *tpst* plants treated with PSK for 11 days to capture late responses to PSK. The roots and shoots were profiled separately to discern possible tissue-specific responses to PSK at different time points (Table 1). I performed additional RNA-seq profiling of 7-day-old *tpst* plants treated with 100 nM or 1 μM PSK for 5 hours and profiled the whole seedlings to investigate potential dose-effects of PSK (Table 1). These diverse experimental settings facilitated a comprehensive understanding of the PSK signaling pathway, allowing me to identify common genes and functional pathways responsive to PSK irrespective of plant age, tissue type, PSK concentration, or duration of treatment.

The principal component analysis demonstrates that the three biological replicates within each group clustered closely together, indicating a high level of reproducibility for both sets of RNA-seq experiments (Figure 8).

group name	library name	organism	tissue	genotype	age	treatment	time
WT_seedling	WT	*Arabidopsis thaliana*	seedling	Col-0	7-day-old	none	0
PSK_0	tpst	*Arabidopsis thaliana*	seedling	*tpst*	7-day-old	none	0
PSK_100nM	PSK	*Arabidopsis thaliana*	seedling	*tpst*	7-day-old	100 nM PSK	5 hours
PSK_1uM	PSK_10x	*Arabidopsis thaliana*	seedling	*tpst*	7-day-old	1 μM PSK	5 hours
WT_shoot	WL_0	*Arabidopsis thaliana*	shoot	Col-0	11-day-old	none	0
shoot_0	TL_0	*Arabidopsis thaliana*	shoot	*tpst*	11-day-old	none	0
shoot_30m	TL_30m	*Arabidopsis thaliana*	shoot	*tpst*	11-day-old	10 nM PSK	30 minutes
shoot_2h	TL_2h	*Arabidopsis thaliana*	shoot	*tpst*	11-day-old	10 nM PSK	2 hours
shoot_5h	TL_5h	*Arabidopsis thaliana*	shoot	*tpst*	11-day-old	10 nM PSK	5 hours
shoot_11d	TL_11d	*Arabidopsis thaliana*	shoot	*tpst*	11-day-old	10 nM PSK	11 days
WT_root	WR_0	*Arabidopsis thaliana*	root	Col-0	11-day-old	none	0
root_0	TR_0	*Arabidopsis thaliana*	root	*tpst*	11-day-old	none	0
root_30m	TR_30m	*Arabidopsis thaliana*	root	*tpst*	11-day-old	10 nM PSK	30 minutes
root_2h	TR_2h	*Arabidopsis thaliana*	root	*tpst*	11-day-old	10 nM PSK	2 hours
root_5h	TR_5h	*Arabidopsis thaliana*	root	*tpst*	11-day-old	10 nM PSK	5 hours
root_11d	TR_11d	*Arabidopsis thaliana*	root	*tpst*	11-day-old	10 nM PSK	11 days

Table 1. Information of each plant sample and PSK treatment in RNA-seq experiments. Group name of the plant sample was used in differential expression analysis, functional enrichment analysis and transcription factors enrichment analysis. Library name of the plant sample was used in principal component analysis and data submission to Gene Expression Omnibus.

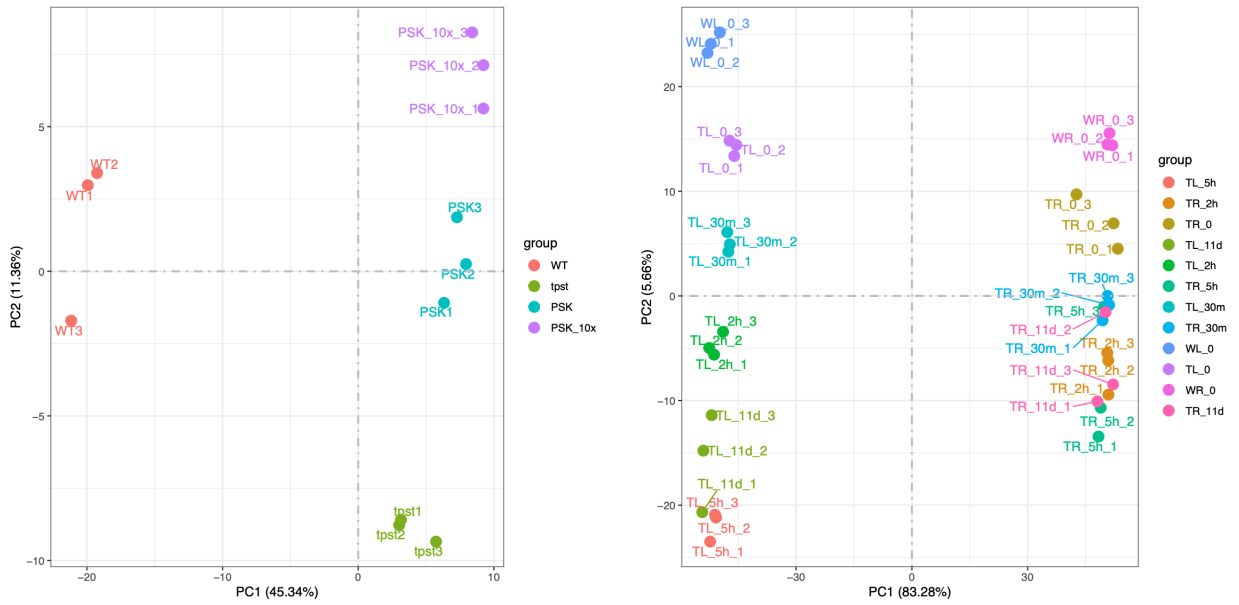

Figure 8. Principle component analysis of the two sets of RNA-seq experiments. The left side shows the analysis of whole seedlings and the right side shows the time course and tissue type analysis. Each color represents the three biological replicates within specific group. The spatial proximity of the biological replicates indicate similarity in transcriptomics.

2.2 Differential expression analysis reveals the number of differentially expressed genes in response to PSK

Differential expression analysis was conducted by comparing WT plants and treated *tpst* plants with untreated or mock-treated *tpst* plants with the cut-off of ≥ 2-fold change and adjusted p-value < 0.05 to identify genes with significant changes in response to PSK. I observed that longer exposure to PSK generally induced a larger magnitude of transcriptional changes, and shoots exhibited a higher number of differentially expressed genes (DEGs) compared to roots at the same time points (Figure 9). When profiling whole seedlings, a higher concentration of PSK led to a greater number of DEGs, indicating a dose effect of PSK. However, the magnitude of

transcriptional changes was smaller compared to profiling roots and shoots separately with plants at a later stage (Figure 9).

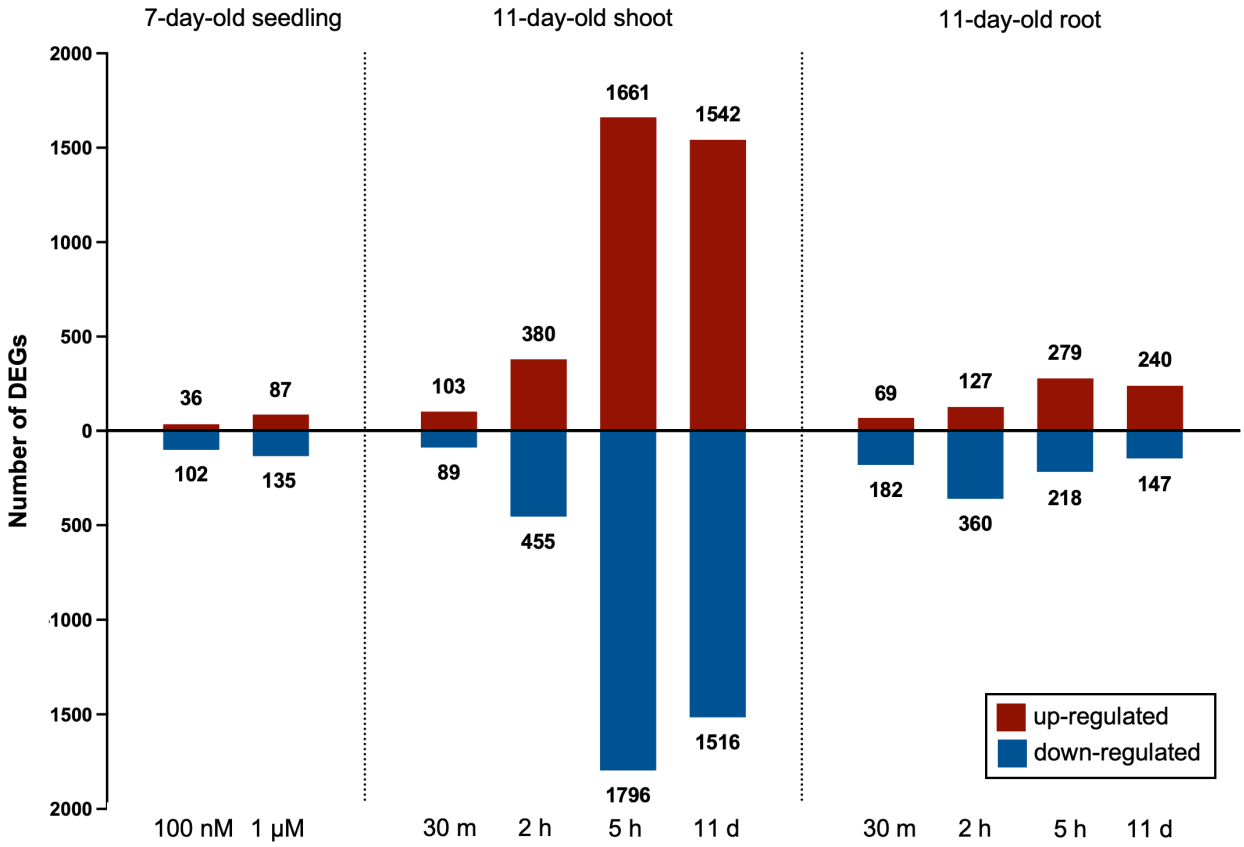

Figure 9. Number of Differentially Expressed Genes (DEGs) after PSK treatments. Differential expression analysis was conducted by comparing PSK-treated *tpst* plants with untreated or mock-treated *tpst* plants. Red indicates up-regulated genes, while blue indicates down-regulated genes, using the cut-off of ≥ 2-fold change and adjusted p-value < 0.05.

2.3 Functional enrichment analysis reveals the defense suppression effect of PSK

Functional enrichment analysis is able to determine whether a set of genes shares common functional characteristics or is significantly enriched for particular biological processes, cellular components and molecular functions.

Since PSK promotes growth, I expected to see up-regulation of growth-related genes. Surprisingly, from functional enrichment analysis of DEGs in each PSK treatment and growth condition using the cut-off of q-value < 0.05, growth-related Gene Ontology Biological Process (GO_BP) terms like growth-related GO_BP terms like “plant epidermis development” and “thalianol metabolic process” were only enriched from PSK up-regulated DEGs in seedling samples with a limited number of DEGs (Figure 10). The thalianin pathway is associated with plant growth, and the overexpression of thalianol synthase *THAS* leads to longer roots [25, 26]. The core genes in thalianin pathway were up-regulated by 100 nM and 1 μM PSK when profiled as whole seedling (≥ 2-fold change and adjusted p-value < 0.05; Figure 11). However, these functional terms were not enriched from separately profiled roots and shoots samples from plants at a later stage (Figure 10, Cluster 1). Instead, hypoxia response-related GO_BP terms like “response to hypoxia”, “anaerobic respiration” enriched from PSK up-regulated DEGs were more commonly shared among different PSK treatment conditions, suggesting PSK has a wide up-regulation effect on the expression of hypoxia-related genes (Figure 10, Cluster 2, 4).

Numerous defense-related GO_BP terms such as “defense response to bacterium”, “regulation of defense response”, “immune system process”, along with important defense-related hormone pathways such as “response to salicylic acid”, “response to jasmonic acid” were enriched from PSK down-regulated DEGs. These defense-associated functional terms were widely shared among various PSK treatment conditions (Figure 12, Cluster 3, 4). Many important genes related to plant defense response, such as *FOX1*, *FOX5*, *MLO12*, *PCR8*, *IOS1*, *WRKY22*, *WRKY 72*, and *PME41* were significantly down-regulated by PSK (≥ 2-fold change and adjusted p-value < 0.05; Figure 11).

Taken together, the suppression effect of PSK on defense-related genes is more prominent and consistent compared to its activation effect on growth-related genes, both in terms of the number of DEGs and GO_BP terms enriched.

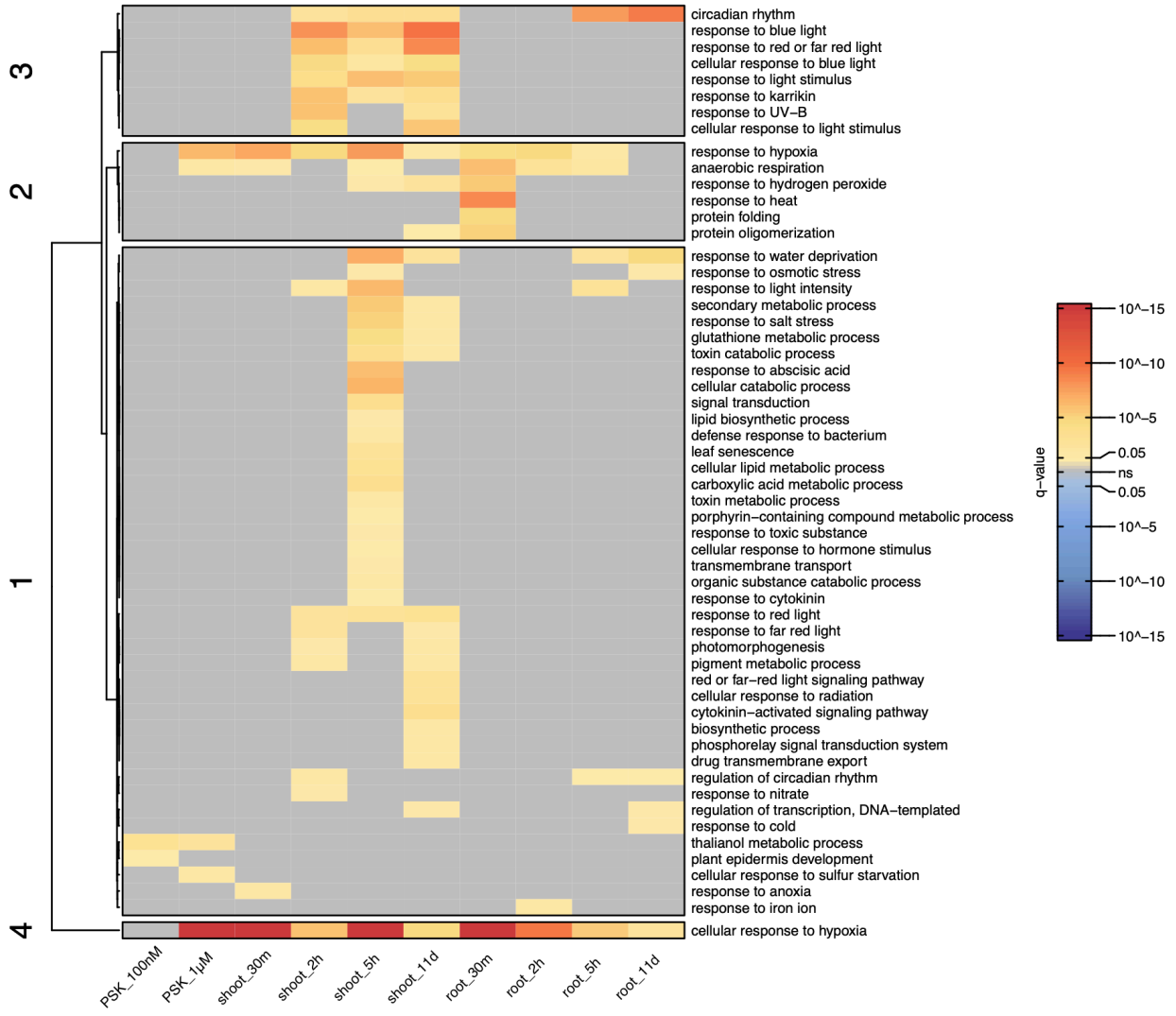

Figure 10. Heatmap of Gene Ontology Biological Process (GO_BP) terms enriched from PSK up-regulated DEGs. The dendrogram on the side of the heatmap illustrates the hierarchical clustering of row using k-means clustering with numbers on the branches denoting the distance measures. The intensity of red reflects their significance measured by q-value, utilizing the cut-off of q-value < 0.05.

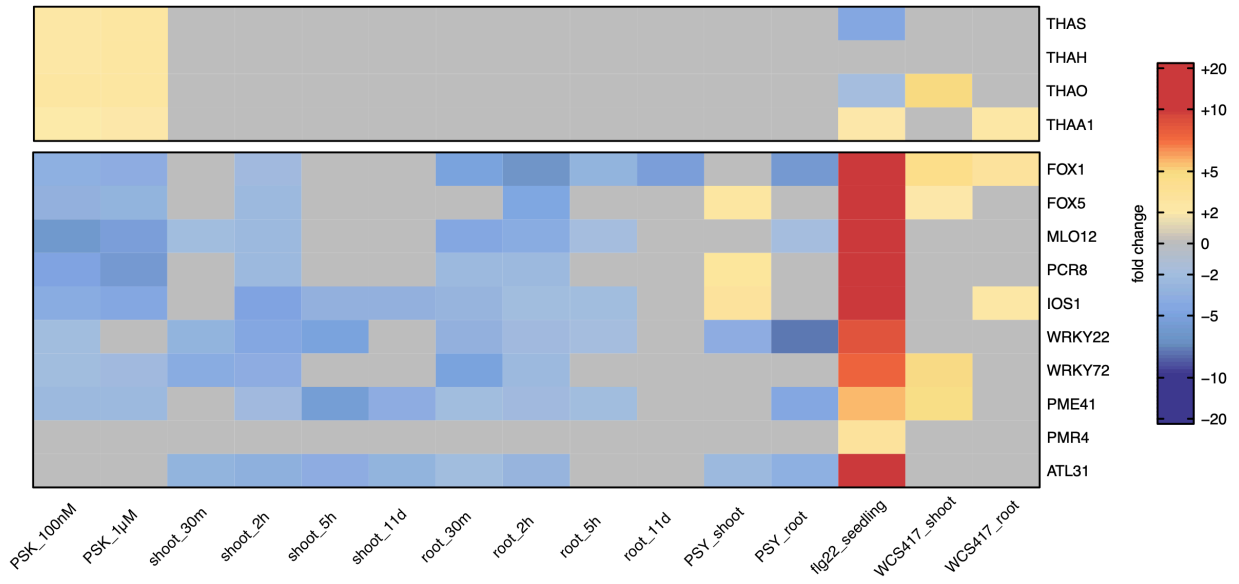

Figure 11. Heatmap of representative differentially expressed genes with PSK, PSY, flg22, and WCS417 treatments. The genes in top section are thalianin pathway-related, and the genes in bottom section are defense-related. Red indicates up-regulation, while blue indicates down-regulation. The intensity of color reflects their fold changes, utilizing the cut-off of $\geq$ 2-fold change and adjusted p-value < 0.05.

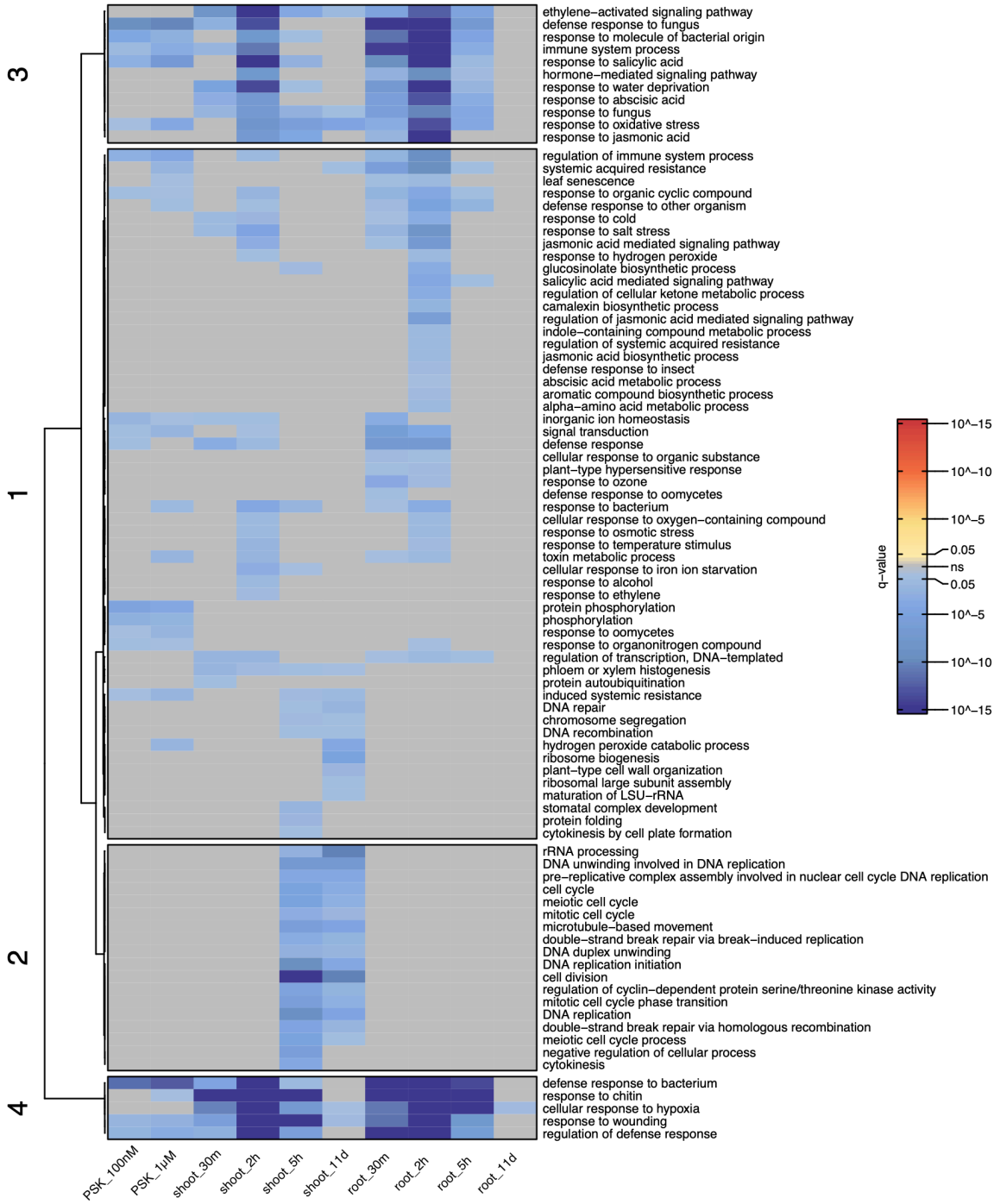

Figure 12. Heatmap of Gene Ontology Biological Process (GO_BP) terms enriched from PSK down-regulated DEGs. The dendrogram on the side of the heatmap illustrates the hierarchical clustering of row using k-means clustering with numbers on the branches denoting the distance measures. The intensity of blue reflects their significance measured by q-value, utilizing the cut-off of q-value < 0.05.

2.4 Transcription factor enrichment analysis indicates WRKY TFs as key regulators in PSK signaling pathway

To identify the transcription factors (TFs) that are likely to regulate PSK-responsive genes, I conducted TF enrichment analysis of DEGs affected by PSK. WRKY TFs account for a significant portion of enriched TFs from PSK down-regulated DEGs, constituting 88.5% to 100% of all enriched TFs in seedling samples, 5.6% to 34.1% in shoot samples, and 25.5% to 81.3% in root samples (Table 2, 3). WRKY TFs are one of the largest transcription factors families in plant and have 75 members in Arabidopsis [27, 28]. WRKY TFs are characterized by the signature 'WRKYGQK' motif at N-termini and a zinc finger motif at C-termini in their DNA-binding domains [27, 28]. WRKY TFs play important roles in regulating plant response to both biotic and abiotic stress and are essential players in plant defense response [29, 30].

Notably, no WRKY TFs were enriched from PSK up-regulated DEGs, except for 2 WRKY TFs identified in root samples exposed to PSK for 11 days. The signature binding motifs of WRKY TFs target genes, W-boxes (TTGACT/TTGACA), were predominantly overrepresented in the promoter regions of PSK down-regulated DEGs, but not in PSK up-regulated DEGs. This aligns with the findings of the TF enrichment analysis (Table 4, 5).

In summary, WRKY TFs play significant regulatory roles in PSK down-regulated DEGs, while not in PSK up-regulated DEGs. Additionally, the *TPST* gene, all *PSK* precursors genes (*PSK1-5*) and *PSK* receptors genes (*PSKR1-2*) possess at least one of the two W-box signature binding motifs in their promoter regions (Table 6). There is experimental evidence that *PSK3, 4, 5* are targeted by WRKY40 and *PSKR1* is targeted by WRKY33 [31], indicating WRKY TFs may directly targets genes that are involved in PSK signaling.

data type	geno type	age	tissue	medium	condition	treatment	concen tration	time	reference
PSK	tpst	7 d	seedling	liquid 0.5x MS	16 h /8 h long day	add peptide	100 nM / 1 μM	5 h	Our data
PSK	tpst	11 d	root / shoot	liquid 0.5x MS	16 h /8 h long day	replace medium	10 nM	30 m / 2 h / 5 h / 11 d	Our data
PSY	tpst	7 d	root / shoot	liquid B5	continuo us light	add peptide	1 μM	7 d	Ogawa-Ohnishi, M. et al. (2022)
flg22	Col-0	12 d	seedling	liquid 1x MS	16 h /8 h long day	replace medium	1 μM	2 h	Birkenbihl, R. P. et al. (2017)
WCS417	Col-0	12 d	root / shoot	Solid 0.5x MS	16 h /8 h long day	contact with root at 5 d	10 ul $2x10^6$ CFU ml^{-1}	7 dpi	Desrut, A. et al. (2020)

Table 2. Growth conditions and treatment methods for RNA-seq data used in the comparison of PSK, PSY, flg22 and WCS417 induced DEGs.

	TF enriched from up-regulated DEGs				TF enriched from down-regulated DEGs			
treatment	all TF	WRKY	percent	p-value	all TF	WRKY	percent	p-value
PSK 100 nM seedling	15	0	0.0%	1	29	29	100.0%	< 2.2e-16
PSK 1 μM seedling	20	0	0.0%	1	26	23	88.5%	< 2.2e-16
PSK shoot 30 m	28	0	0.0%	0.63	44	15	34.1%	4.4e-11
PSK shoot 2 h	52	0	0.0%	0.17	80	26	32.5%	< 2.2e-16
PSK shoot 5 h	70	0	0.0%	0.12	54	3	5.6%	0.49
PSK shoot 11 d	40	0	0.0%	0.41	29	4	13.8%	0.031
PSK root 30 m	45	0	0.0%	0.26	32	26	81.3%	< 2.2e-16
PSK root 2 h	12	0	0.0%	1	51	13	25.5%	5.6e-08
PSK root 5 h	55	0	0.0%	0.17	32	17	53.1%	< 2.2e-16
PSK root 11 d	51	2	4.0%	1	9	7	77.8%	5.7e-09
PSY shoot	13	5	38.5%	0.00011	76	8	10.5%	0.012
PSY root	0	0	0.0%	1	45	27	60.0%	< 2.2e-16
flg22 seedling	77	41	53.2%	< 2.2e-16	123	1	0.1%	0.058
WCS417 shoot	1	0	0.0%	1	8	0	0.0%	1
WCS417 root	39	21	53.8%	< 2.2e-16	12	0	0.0%	1

Table 3. Number of enriched TFs, WRKY TFs, and percentage of WRKY TFs among all TFs from up- or down-regulated DEGs with PSK, PSY, flg22, and WCS417 treatments. The p-value represents Fisher's exact test for the overrepresentation of enriched WRKY TFs among all TFs compared to the genome background.

		W-box motifs in up-regulated DEGs promoter regions (1000 bp upstream)				
treatment	oligomer	N in list	N in genome	% in DEG	% in genome	p-value
PSK 100 nM seedling	TTGACT	28	25580	16/36	17247/34187	0.51
	TTGACC	13	15426	10/36	12035/34187	0.39
PSK 1 µM seedling	TTGACT	62	25580	48/87	17247/34187	0.39
	TTGACC	31	15426	28/87	12035/34187	0.65
PSK shoot 30 m	TTGACT	68	25580	45/103	17247/34187	0.20
	TTGACC	47	15426	35/103	12035/34187	0.84
PSK shoot 2 h	TTGACT	251	25580	183/380	17247/34187	0.38
	TTGACC	139	15426	111/380	12035/34187	0.015
PSK shoot 5h	TTGACT	1266	25580	836/1661	17247/34187	0.94
	TTGACC	754	15426	583/1661	12035/34187	0.94
PSK shoot 11 d	TTGACT	1078	25580	736/1542	17247/34187	0.031
	TTGACC	646	15426	514/1542	12035/34187	0.12
PSK root 30 m	TTGACT	51	25580	34/69	17247/34187	0.90
	TTGACC	31	15426	25/69	12035/34187	0.90
PSK root 2 h	TTGACT	82	25580	54/127	17247/34187	0.076
	TTGACC	46	15426	34/127	12035/34187	0.050
PSK root 5 h	TTGACT	179	25580	124/279	17247/34187	0.047
	TTGACC	106	15426	87/279	12035/34187	0.17
PSK root 11 d	TTGACT	183	25580	118/240	17247/34187	0.70
	TTGACC	100	15426	79/240	12035/34187	0.50
PSY shoot	TTGACT	191	25580	97/161	17247/34187	0.014
	TTGACC	93	15426	65/161	12035/34187	0.19
PSY root	TTGACT	185	25580	128/279	17247/34187	0.13
	TTGACC	104	15426	80/279	12035/34187	0.023
flg22 seedling	TTGACT	4253	25580	2520/4048	17247/34187	< 2.2e-16
	TTGACC	2590	15426	1843/4048	12035/34187	< 2.2e-16
WCS417 shoot	TTGACT	692	25580	411/694	17247/34187	3.3e-06
	TTGACC	386	15426	289/694	12035/34187	0.00040
WCS417 root	TTGACT	1056	25580	627/1002	17247/34187	5.0e-15
	TTGACC	558	15426	414/1002	12035/34187	4.8e-05

Table 4. Number of W-box motifs in the promoter regions (1000 bp upstream) of up-regulated DEGs, number of W-box motifs in the promoter regions of all genes in the genome, percentage of DEGs containing W-box motifs among all DEGs, and percentage of genes containing W-box motifs among all genes in each treatment condition. The p-value represent Fisher's exact test for the overrepresentation of DEGs containing W-box motifs compared to the genome background.

		W-box motifs in down-regulated DEGs promoter regions (1000 bp upstream)				
treatment	oligomer	N in list	N in genome	% in DEG	% in genome	p-value
PSK 100 nM seedling	TTGACT	164	25580	78/102	17247/34187	8.2e-08
	TTGACC	71	15426	50/102	12035/34187	0.0048
PSK 1 µM seedling	TTGACT	194	25580	91/135	17247/34187	9.0e-05
	TTGACC	83	15426	60/135	12035/34187	0.030
PSK shoot 30 m	TTGACT	140	25580	69/89	17247/34187	1.9e-07
	TTGACC	57	15426	39/89	12035/34187	0.096
PSK shoot 2 h	TTGACT	518	25580	288/455	17247/34187	3.7e-08
	TTGACC	257	15426	182/455	12035/34187	0.034
PSK shoot 5h	TTGACT	1443	25580	933/1796	17247/34187	0.20
	TTGACC	835	15426	644/1796	12035/34187	0.56
PSK shoot 11 d	TTGACT	1227	25580	789/1516	17247/34187	0.21
	TTGACC	728	15426	568/1516	12035/34187	0.061
PSK root 30 m	TTGACT	275	25580	137/182	17247/34187	8.5e-12
	TTGACC	155	15426	105/182	12035/34187	6.6e-10
PSK root 2 h	TTGACT	451	25580	243/360	17247/34187	6.7e-11
	TTGACC	284	15426	187/360	12035/34187	8.0e-11
PSK root 5 h	TTGACT	264	25580	139/218	17247/34187	7.6e-05
	TTGACC	133	15426	90/218	12035/34187	0.064
PSK root 11 d	TTGACT	183	25580	89/147	17247/34187	0.016
	TTGACC	79	15426	54/147	12035/34187	0.73
PSY shoot	TTGACT	401	25580	240/418	17247/34187	0.0043
	TTGACC	207	15426	149/418	12035/34187	0.88
PSY root	TTGACT	817	25580	460/713	17247/34187	2.6e-14
	TTGACC	429	15426	302/713	12035/34187	7.2e-05
flg22 seedling	TTGACT	1721	25580	1249/2774	17247/34187	2.7e-09
	TTGACC	1084	15426	888/2774	12035/34187	0.00024
WCS417 shoot	TTGACT	266	25580	178/381	17247/34187	0.15
	TTGACC	165	15426	123/381	12035/34187	0.24
WCS417 root	TTGACT	329	25580	216/454	17247/34187	0.22
	TTGACC	183	15426	146/454	12035/34187	0.18

Table 5. Number of W-box motifs in the promoter regions (1000 bp upstream) of down-regulated DEGs, number of W-box motifs in the promoter regions of all genes in the genome, percentage of DEGs containing W-box motifs among all DEGs, and percentage of genes containing W-box motifs among all genes in each treatment condition. The p-value represent Fisher's exact test for the overrepresentation of DEGs containing W-box motifs compared to the genome background.

Gene ID	Gene name	TTGACT in promotor region	TTGACC in promoter region
AT1G08030	TPST	×	√
AT1G13590	PSK1	√	×
AT2G22860	PSK2	√	×
AT3G44735	PSK3	√	×
AT3G49780	PSK4	√	√
AT5G65870	PSK5	√	√
AT2G02220	PSKR1	√	×
AT5G53890	PSKR2	√	×

Table 6. The presence of W-box motifs in the promoter regions of genes involved in PSK signaling.

2.5 WRKY TFs in ATRM map

The Arabidopsis Transcriptional Regulatory Map (ATRM) provides a high-quality Arabidopsis transcriptional regulatory map that covers 388 TFs with strong supporting evidence from published references [32]. Degree centrality measures the number of neighbors each node has and closeness centrality measures the impact of a certain node in biological networks [33]. By integrating ATRM's manually curated high-confidence dataset, I was able to assess the degree centrality and closeness centrality of WRKY TFs among these annotated TFs (Figure 13). Most WRKY TFs within this network exhibited relatively high levels of degree centrality, suggesting they are among the transcription factors with the most interconnected nodes. Additionally, they displayed very high levels of closeness centrality, indicating their roles as rapid communicators within the network. This observation aligns with our findings from the TF enrichment analysis, highlighting the influential impact of WRKY TFs in the regulatory network.

I integrated regulatory effects from the ATRM dataset and constructed a regulatory network for WRKY TFs (Figure 14). Many important plant defense genes in this network, such as

PR1, *FRK1*, *AOS*, *LOX2*, *LOX3*, *PDF1.2*, *BGL2*, *LURP1*, *ORA59*, *ERF1*, *ERF4*, *HSFB2A*, and *HSFB2B*, are regulated by WRKY TFs, and they were down-regulated by PSK (Figure 15, 16), indicating WRKY TFs' role in PSK-mediated defense gene suppression.

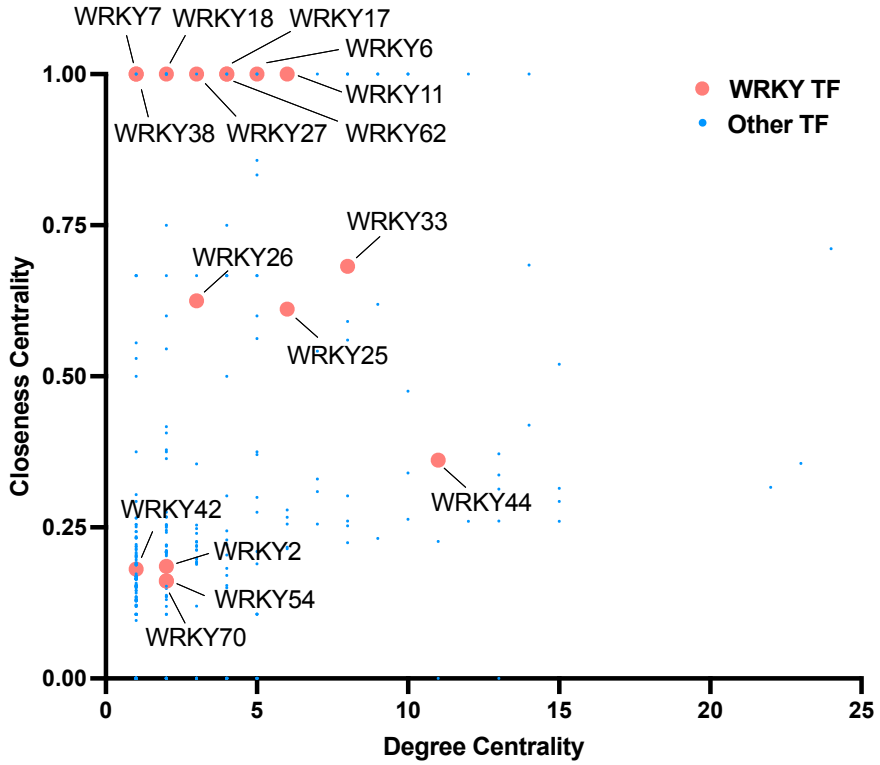

Figure 13. Degree centrality and closeness centrality of manually curated high-confidence TFs from Arabidopsis Transcriptional Regulatory Map (ATRM). Red dots indicate WRKY TFs, blue dots indicate all other TFs.

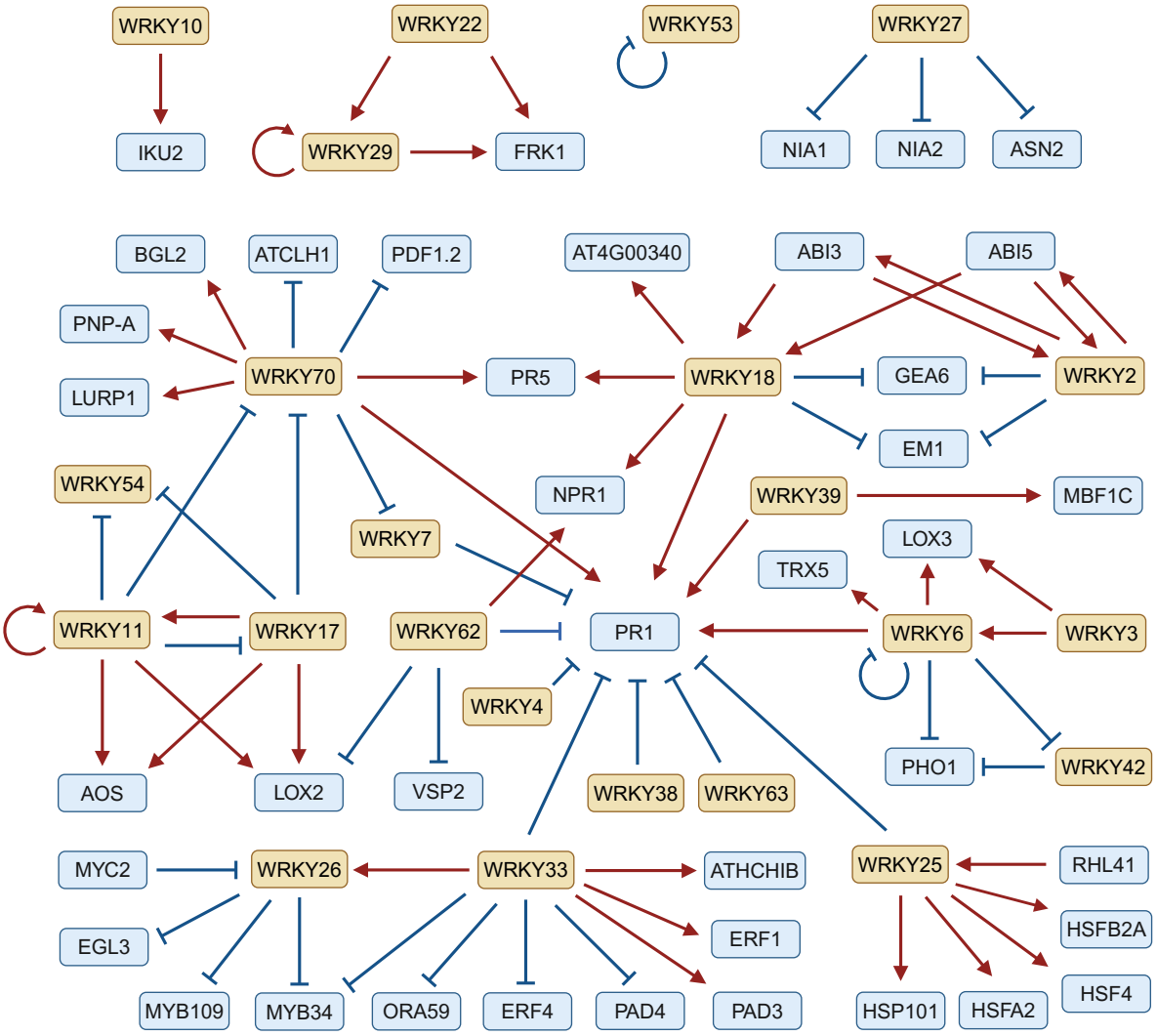

Figure 14. WRKY regulatory network derived from ATRM. Red arrows indicate activation effects, blue ended-lines indicate repression effects.

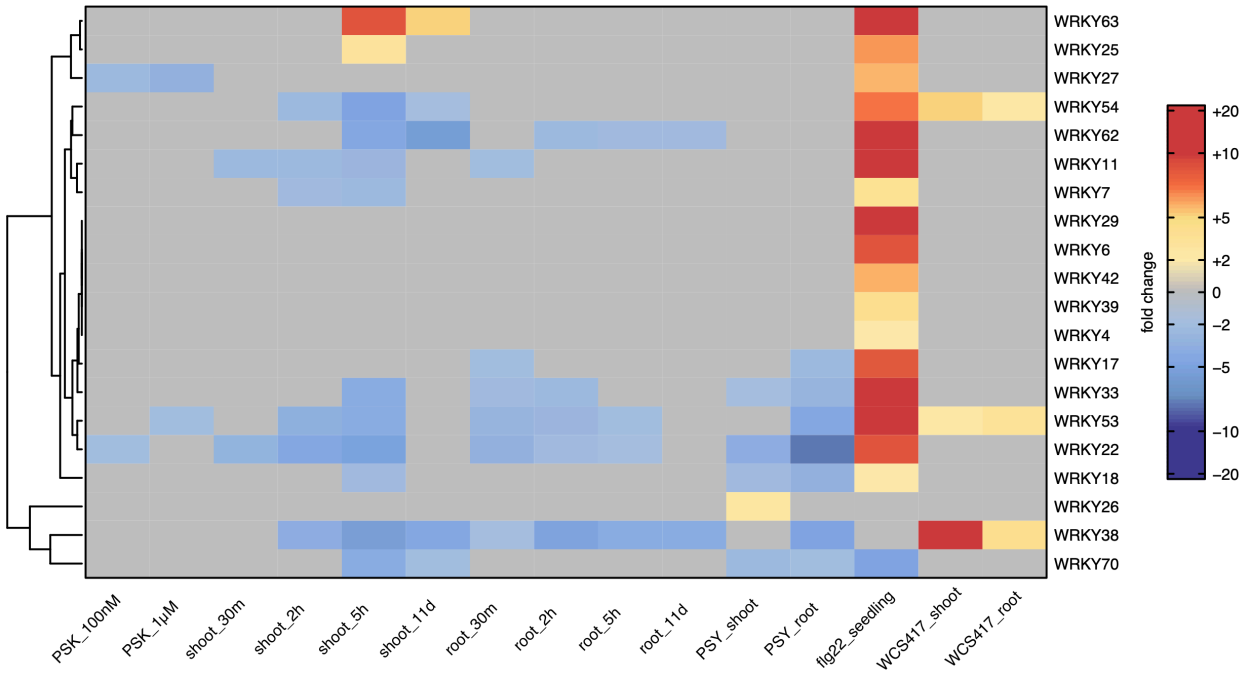

Figure 15. Heatmap of representative differentially expressed WRKY TFs in ATRM map with PSK, PSY, flg22, and WCS417 treatments. The dendrogram on the side of the heatmap illustrates the hierarchical clustering of row using k-means clustering. Red indicates up-regulation, while blue indicates down-regulation. The intensity of color reflects their fold changes, utilizing the cut-off of ≥ 2-fold change and adjusted p-value < 0.05.

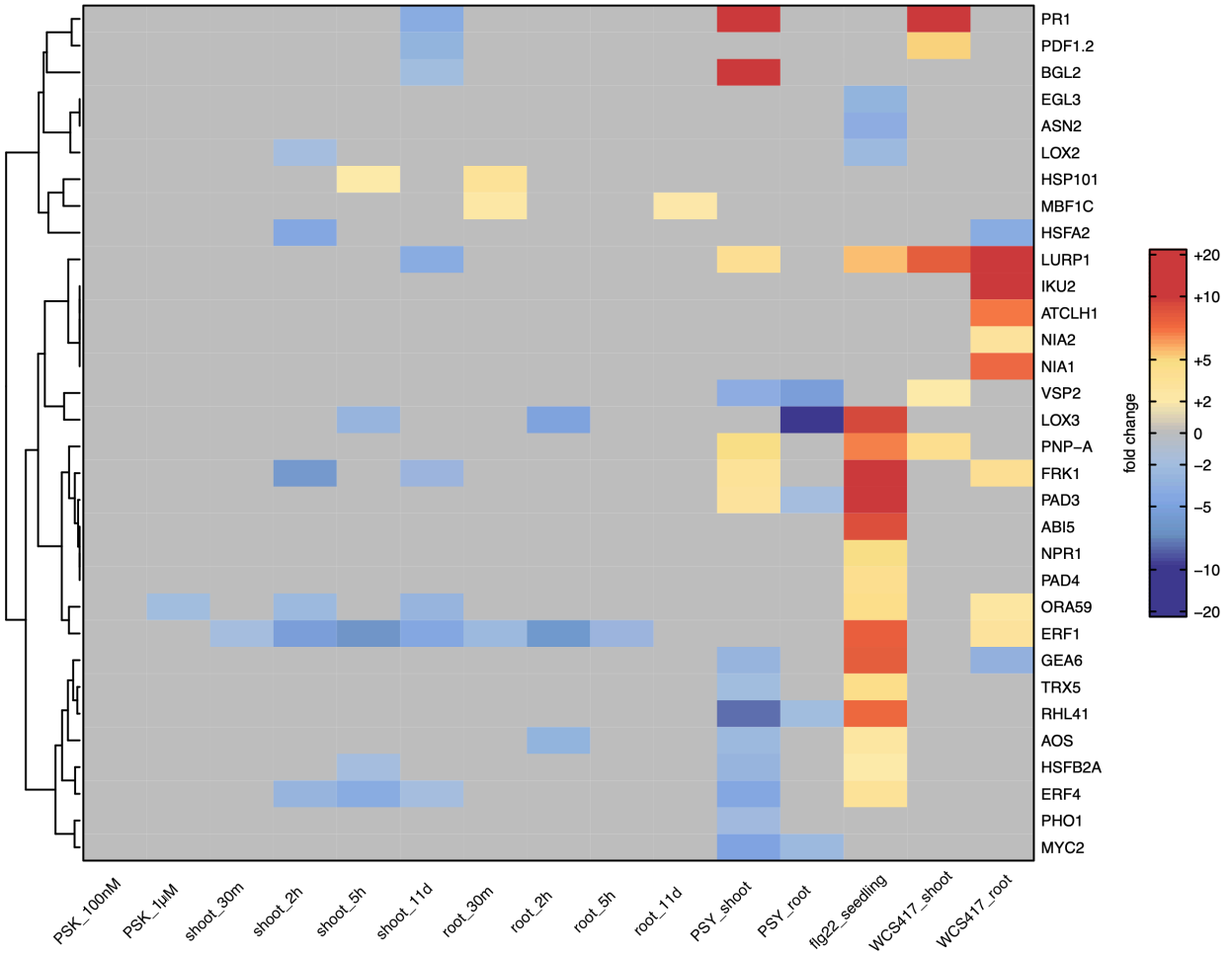

Figure 16. Heatmap of representative differentially expressed genes downstream of WRKY TFs in ATRM map with PSK, PSY, flg22, and WCS417 treatments. The dendrogram on the side of the heatmap illustrates the hierarchical clustering of row using k-means clustering. Red indicates up-regulation, while blue indicates down-regulation. The intensity of color reflects their fold changes, utilizing the cut-off of ≥ 2-fold change and adjusted p-value < 0.05.

2.5 Comparative transcription factor analysis with PSY, flg22, and WCS417

Flagellin 22 (flg22), a pathogen-associated molecular pattern (PAMP) derived from bacterial flagellin, induces dramatic plant defense response. It is also associated with WRKY TFs, but it inhibits plant growth [31]. Considering PSK's suppression effect on plant defense, I wanted

to further investigate whether PSK and flg22 affect a same set of WRKY TFs and defense-associated genes. Additionally, I integrated published RNA-seq data from plants treated with PSY [34], another TPST-sulfated growth-promoting peptide, and *P. simaie* strain WCS417 [35], a beneficial bacterial that promotes plant growth, in addition to flg22, to elucidate their effects on WRKY TFs and plant defense.

TF enrichment analysis revealed that the majority of WRKY TFs were exclusively enriched from down-regulated DEGs of PSK and PSY treatments, and from up-regulated DEGs of flg22 and WCS417 treatments, not vice versa (Figure 17, 18). Furthermore, at the gene expression level, most *WRKY* TF genes were down-regulated by PSK and PSY, but up-regulated by flg22 and WCS417 (Figure 19). The significant overlap observed between any two of the differentially expressed WRKY TFs from PSK, PSY, flg22, and WCS417 treatments, as well as WRKY TFs enriched from DEGs in each case, underscores the existence of a common regulatory network underlying these four distinct pathways, rather than a mere coincidental sharing of a similar set of WRKY TFs (Figure 20, 21, Table 8, 9).

WRKY TFs are a distinctive cluster of all enriched TFs from DEGs of PSK, PSY, flg22, and WCS417 treatments (Figure 17, Cluster 1). The overrepresentation of WRKY TFs and the presence of the WRKY TFs' signature W-box motif also conformed to the observed pattern of "same WRKY TFs but opposite directions" (Table 3, 4, 5). Specifically, WRKY TFs associated with PSK and PSY treatments are predominantly overrepresented in down-regulated DEGs, whereas they are primarily enriched from up-regulated DEGs with flg22 and WCS417 treatments.

Figure 17. Heatmap of all enriched TFs

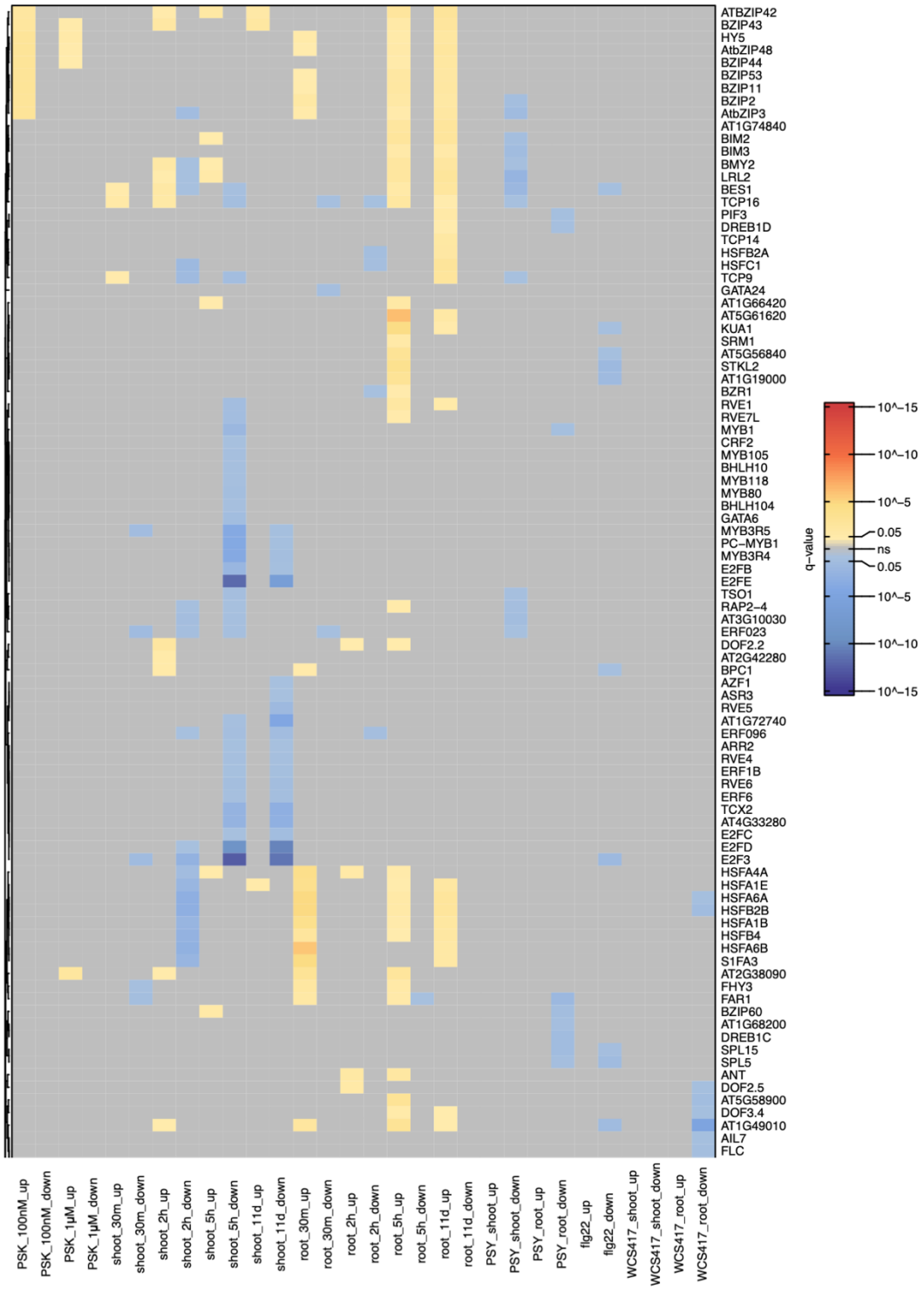

Figure 17. Heatmap of all enriched TFs, continued

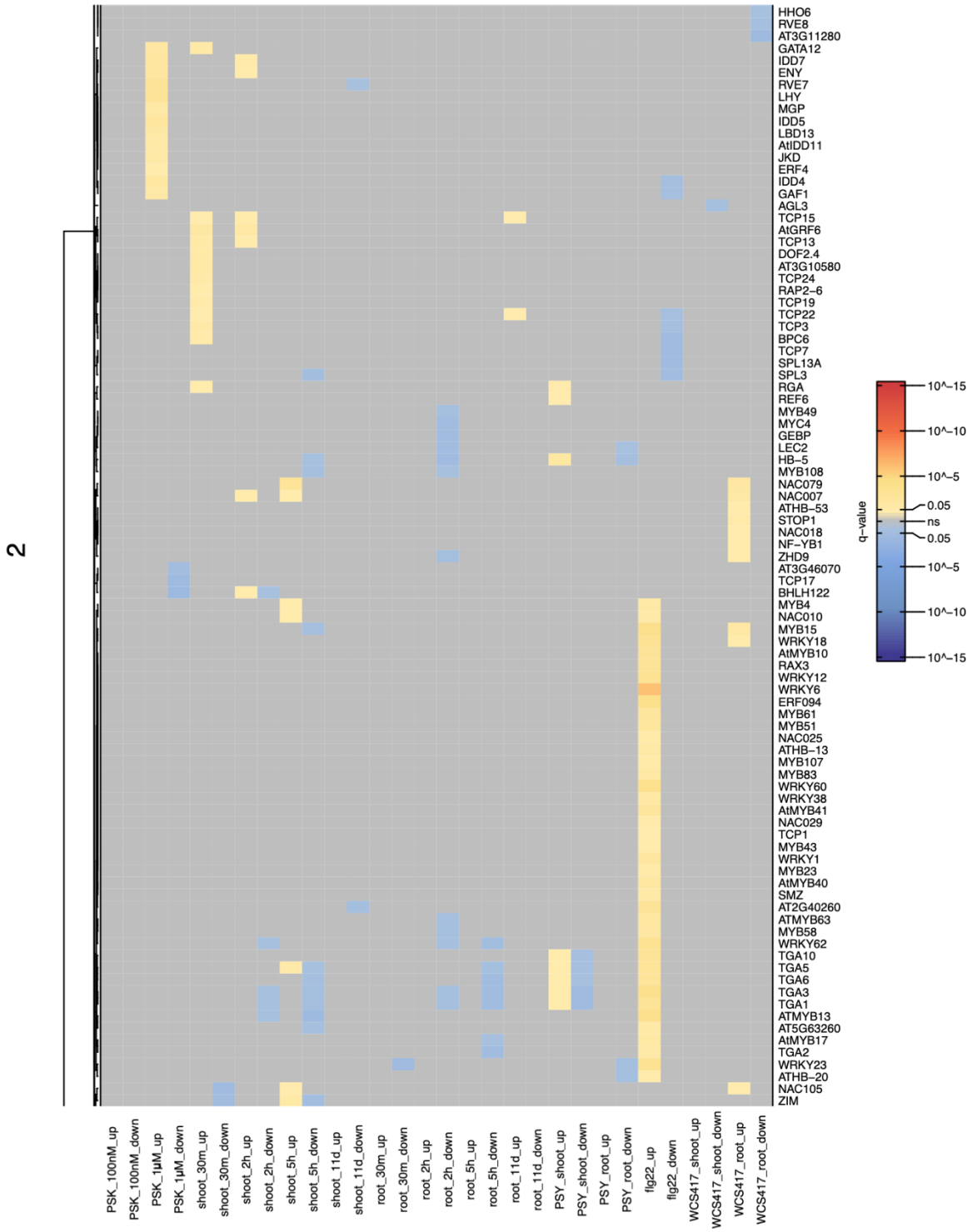

Figure 17. Heatmap of all enriched TFs, continued

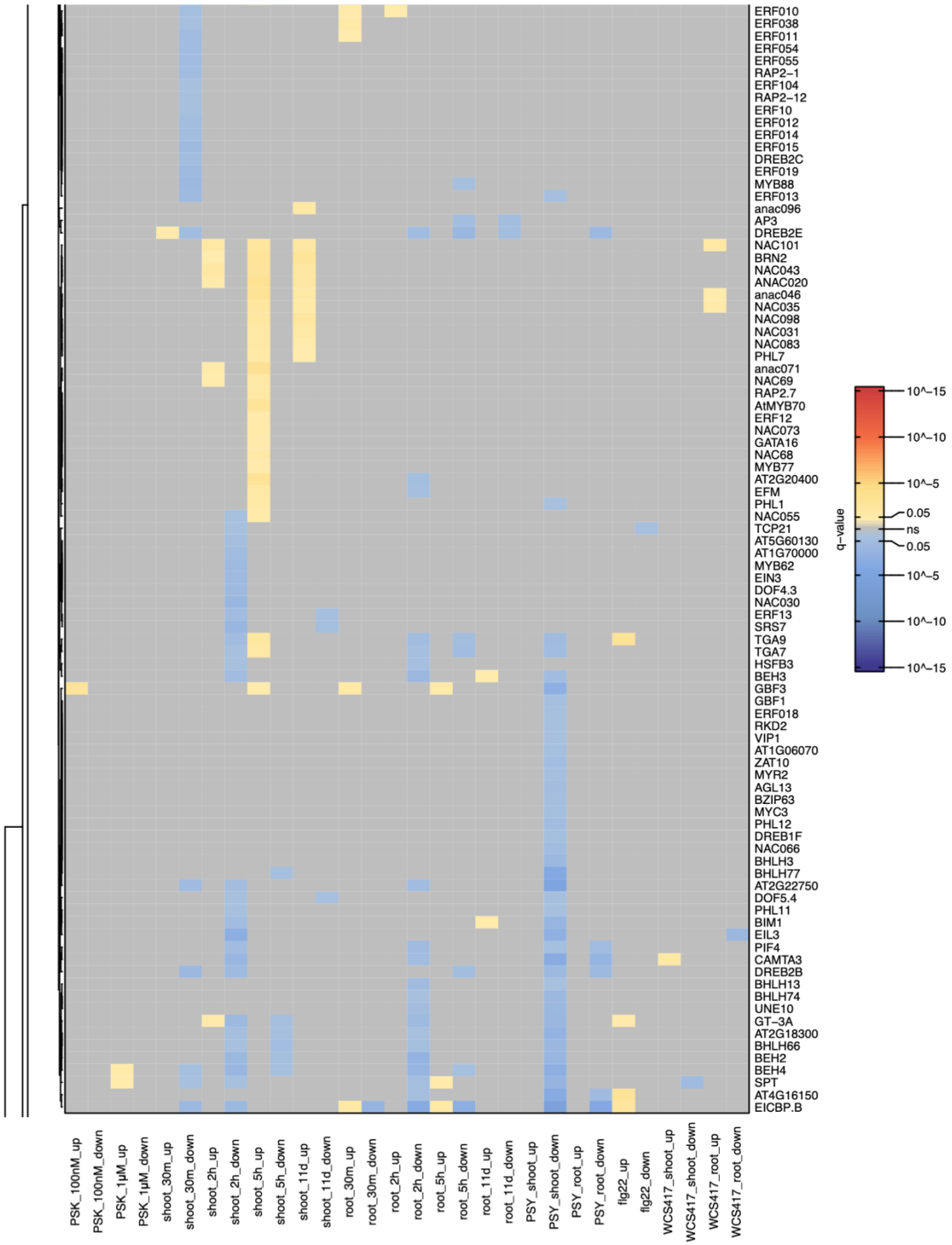

Figure 17. Heatmap of all enriched TFs, continued

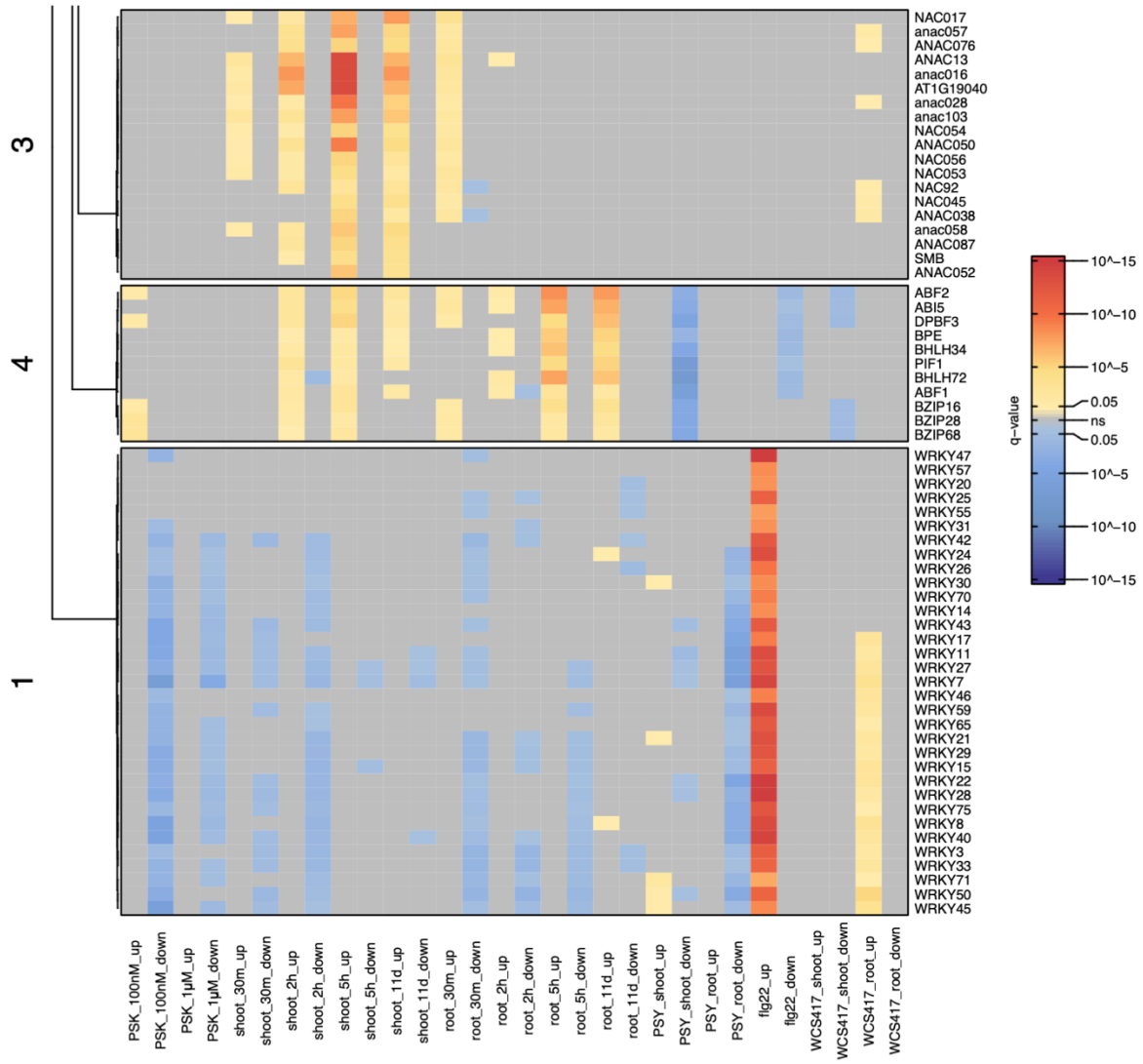

Figure 17. Heatmap of all enriched TFs from PSK, PSY, flg22, and WCS417 up- and down-regulated DEGs. The dendrogram on the side of the heatmap illustrates the hierarchical clustering of row using k-means clustering with numbers on the branches denoting the distance measures. Red denotes enrichment from up-regulated DEGs, while blue denotes enrichment from down-regulated DEGs. The intensity of color reflects their significance measured by q-value, utilizing the cut-off of q-value < 0.05.

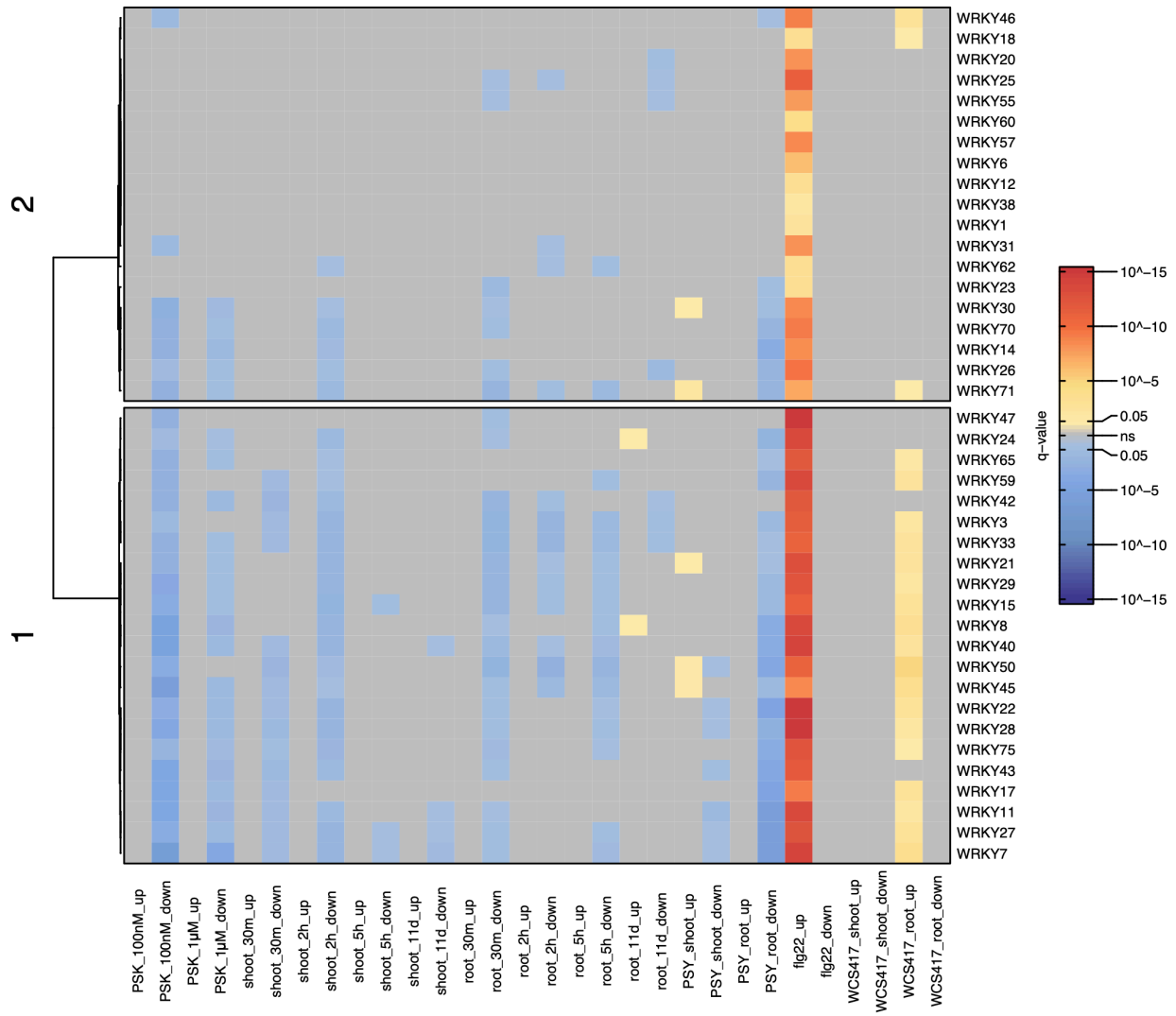

Figure 18. Heatmap of enriched WRKY TFs from PSK, PSY, flg22, and WCS417 up- and down-regulated DEGs. The dendrogram on the side of the heatmap illustrates the hierarchical clustering of row using k-means clustering with numbers on the branches denoting the distance measures. Red denotes enrichment from up-regulated DEGs, while blue denotes enrichment from down-regulated DEGs. The intensity of color reflects their significance measured by q-value, utilizing the cut-off of q-value < 0.05.

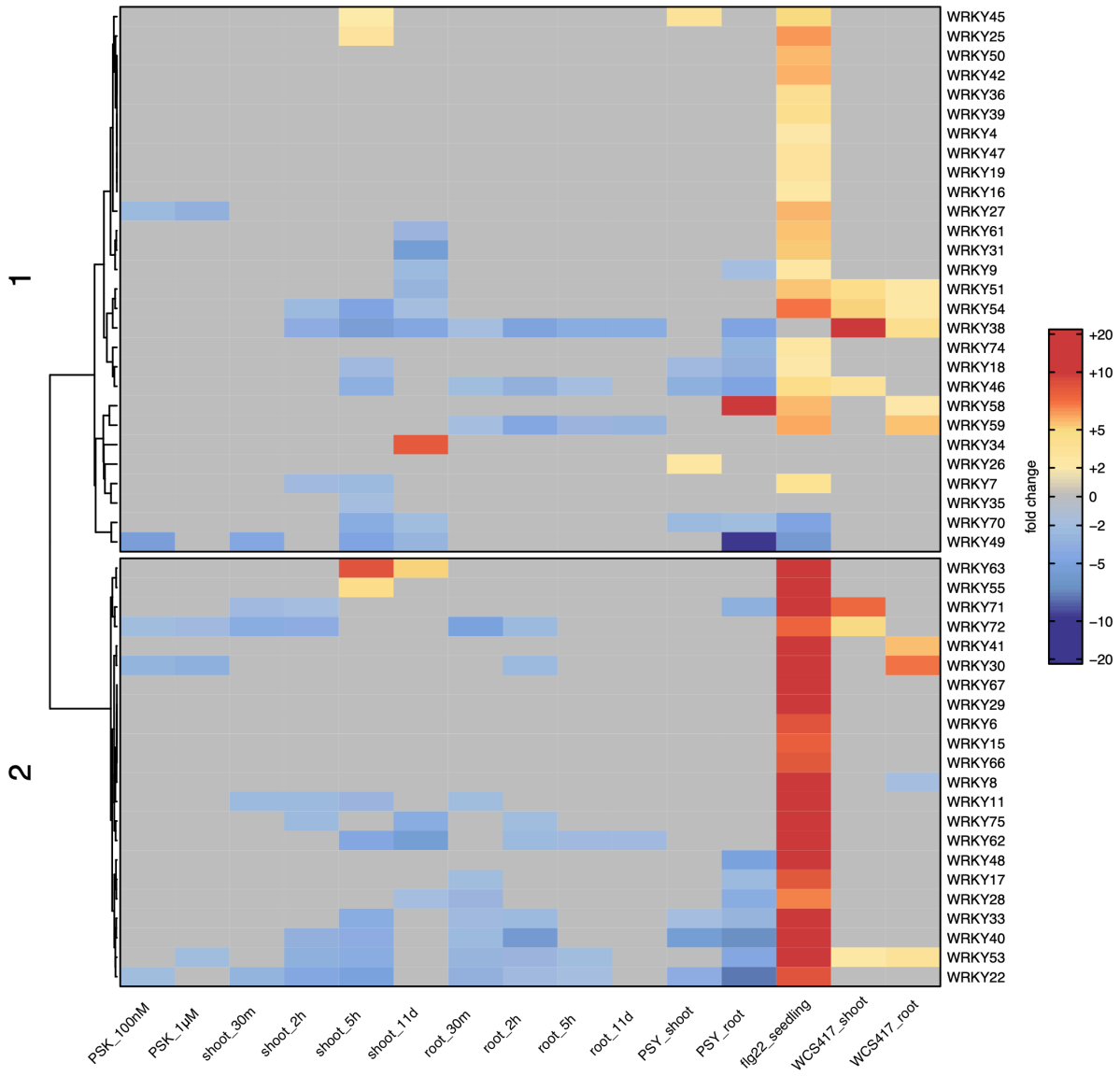

Figure 19. Heatmap of differentially expressed WRKY TFs with PSK, PSY, flg22, and WCS417 treatments. The dendrogram on the side of the heatmap illustrates the hierarchical clustering of row using k-means clustering with numbers on the branches denoting the distance measures. Red indicates up-regulation, while blue indicates down-regulation. The intensity of color reflects their fold changes, utilizing the cut-off of ≥ 2-fold change and adjusted p-value < 0.05.

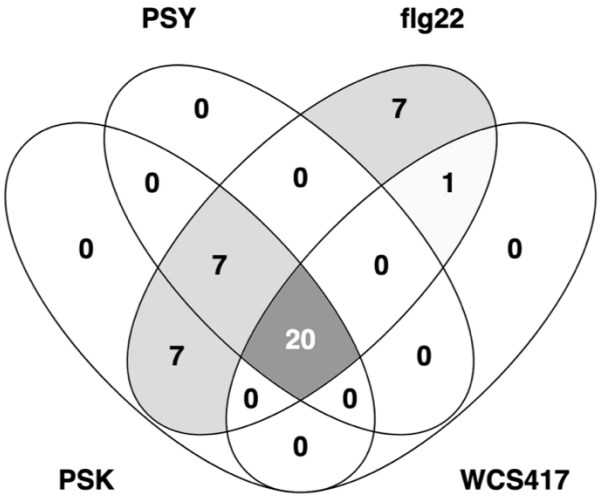

Figure 20. Venn diagram of the number of WRKY TFs enriched from DEGs in PSK, PSY, flg22 and WCS417 treatments.

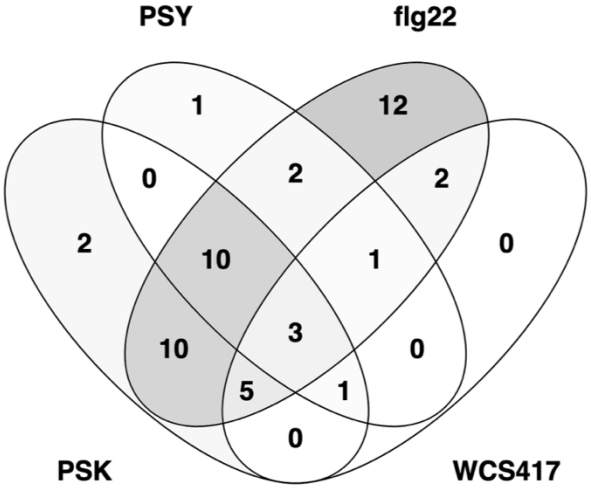

Figure 21. Venn diagram of the number of differentially expressed WRKY TFs in PSK, PSY, flg22 and WCS417 treatment conditions.

	Enriched WRKY TFs in all enriched TFs				Differentially expressed WRKY TFs in all DEGs			
treatment	number	ratio	background	p-value	number	ratio	background	p-value
PSK	34	34/72	279/1717	2.9e-10	31	31/72	5196/32833	3.6e-08
PSY	27	27/72	111/1717	1.5e-15	18	18/72	1382/32833	7.4e-10
flg22	42	42/72	196/1717	< 2.2e-16	45	45/72	6823/32833	1.9e-14
WCS417	21	21/72	60/1717	1.3e-15	12	12/72	2304/32833	0.0041

Table 7. Summary of the total number of enriched WRKY TFs from DEGs in PSK, PSY, flg22 and WCS417 treatments and their ratio over all WRKY TFs in the genome. The background shows the ratio of the total number of enriched TFs over all TFs in the genome. The p-value represents Fisher's exact test for the overrepresentation of enriched WRKY TFs among all WRKY TFs compared to all enriched TFs among the genome background.

	Enriched WRKY TFs in all enriched TFs				Differentially expressed WRKY TFs in all DEGs			
comparison	left	overlap	right	p-value	left	overlap	right	p-value
PSK ∩ PSY	34	27	27	< 2.2e-16	31	14	18	0.00076
PSK ∩ flg22	34	34	42	< 2.2e-16	31	28	45	1.8e-05
PSK ∩ WCS417	34	20	21	1.0e-06	31	9	12	0.017
PSY ∩ flg22	27	27	42	< 2.2e-16	18	16	45	0.0063
PSY ∩ WCS417	27	20	21	< 2.2e-16	18	4	12	0.34
flg22 ∩ WCS417	42	21	21	< 2.2e-16	45	11	12	0.019

Table 8. Number of overlapping enriched WRKY TFs and differentially expressed WRKY TFs shared by PSK, PSY, flg22 and WCS417 treatments. The p-value represents the likelihood of the simulation of randomly selecting the desired number of WRKY TFs from all WRKY TFs in left or right category and having at least the desired number of overlapping, given the hypothesis that they are independent.

2.6 Comparative functional enrichment analysis with PSY, flg22, and WCS417

The overlapping GO_BP terms among PSK, PSY, flg22 and WCS417 treatments predominantly pertain to defense-related response, such as "defense response to bacterium", "regulation of defense response", "response to molecule of bacterial origin", as well as other

defense-related hormone or signaling pathways like “response to salicylic acid”, “response to jasmonic acid”, and “systemic acquired resistance” (Figure 22). Collectively, these findings indicate that PSK and PSY suppress plant defense responses, while flg22 and WCS417 induce plant defense responses, thus corroborating our previous understanding of the distinct effects of these four treatments and pathways [36-38].

Notably, the results of treatment with PSK were more similar to that of PSY treatment in terms of exhibiting fewer DEGs in opposite directions (Figure 23) and inducing similar down-regulation effects on plant defense compared to flg22 and WCS417 (Figure 22). However, the GO_BP terms such as “protein phosphorylation” (Figure 22), GO_CC terms “extracellular region”, “plasma membrane”, “integral component of membrane” (Figure 24), GO_MF terms like “kinase activity”, “ATP binding” (Figure 25) do not align with this pattern. The effects of treatment with PSY were more similar to flg22 and WCS417 treatments, respectively, in terms of up-regulating associated genes linked to these functional terms, whereas PSK down-regulated them. This indicates the existence of mechanistic differences among the response pathways to these four stimuli.

Figure 22. Heatmap of all enriched GO_BP terms

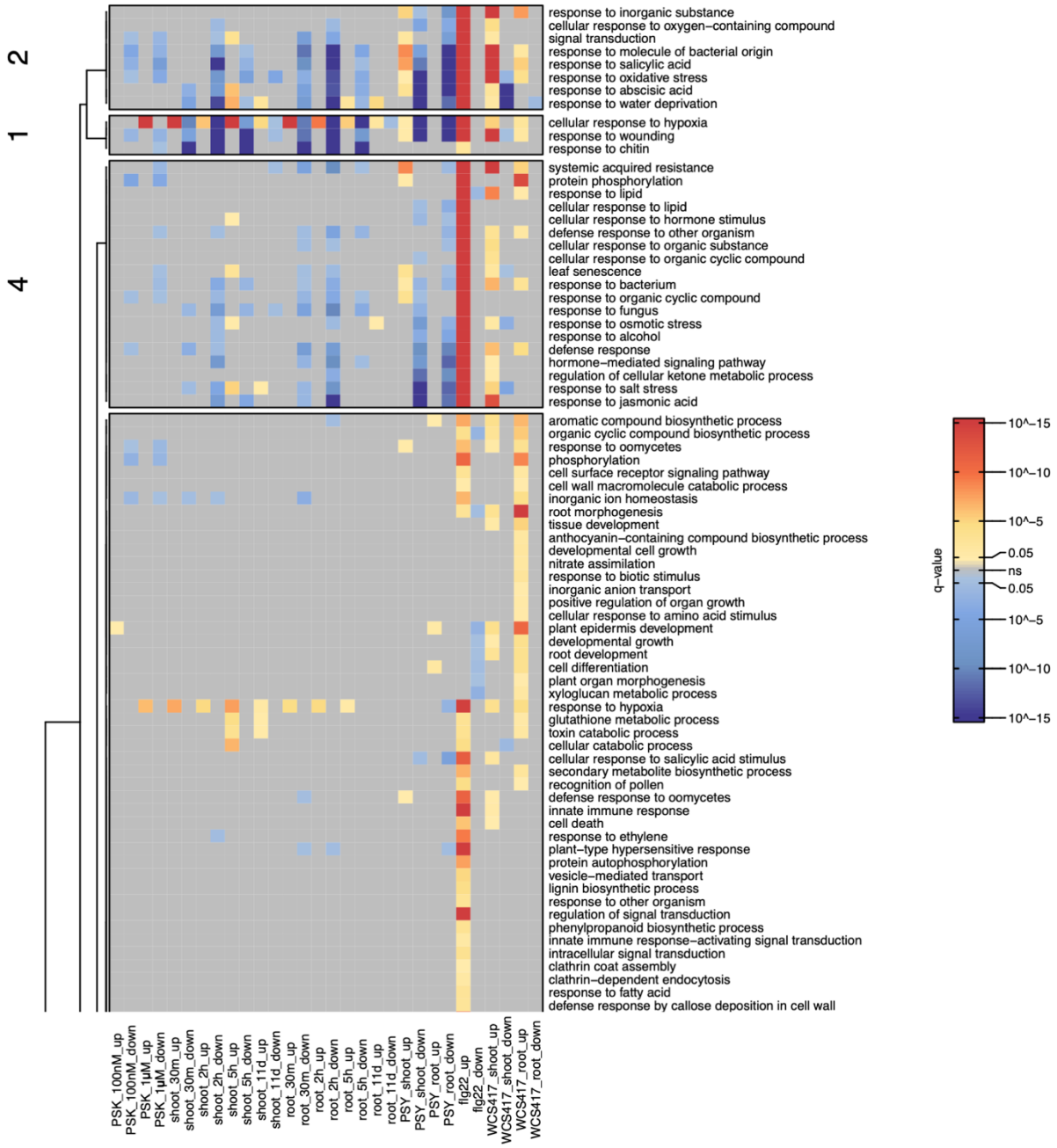

Figure 22. Heatmap of all enriched GO_BP terms, continued

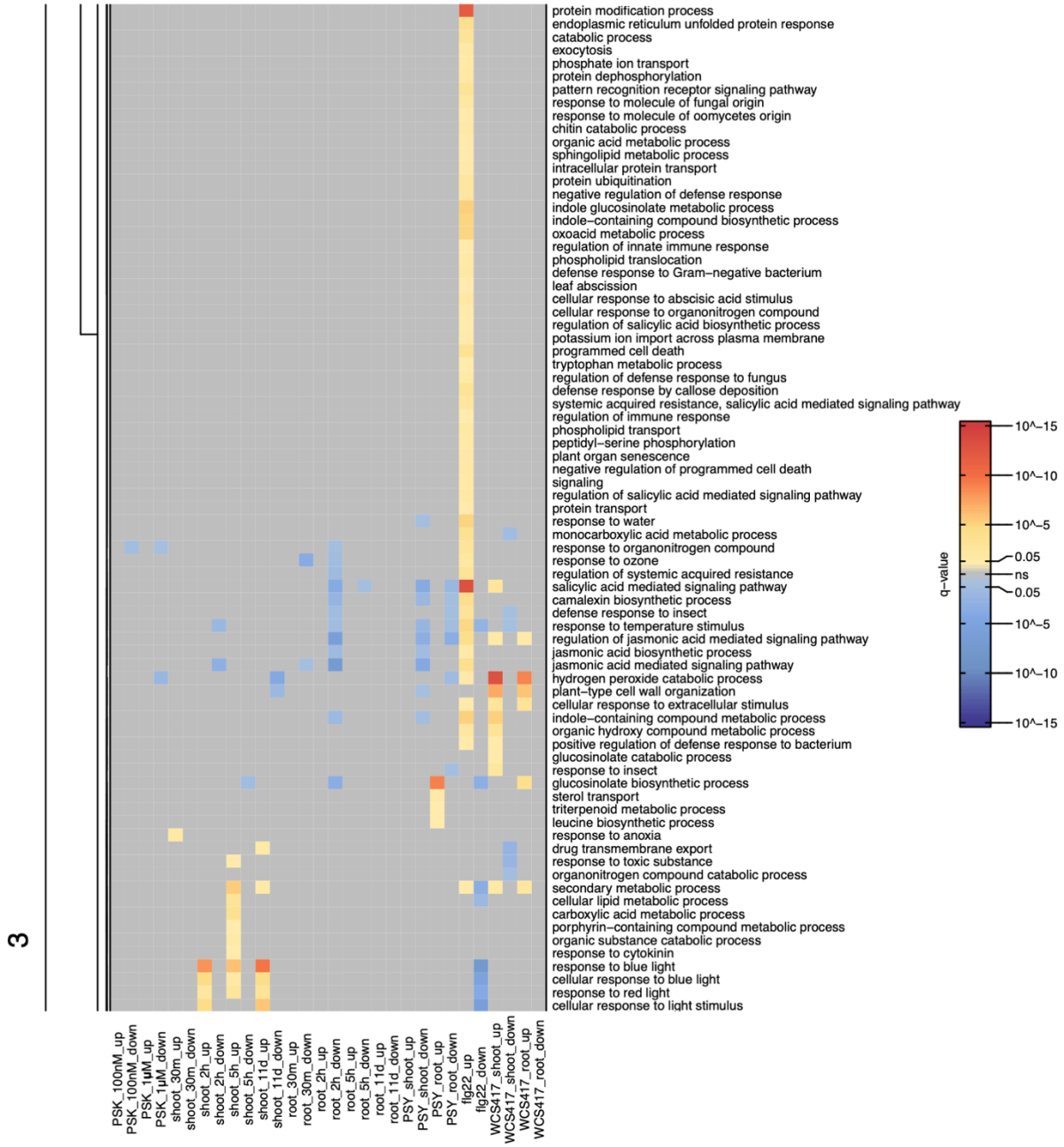

Figure 22. Heatmap of all enriched GO_BP terms, continued

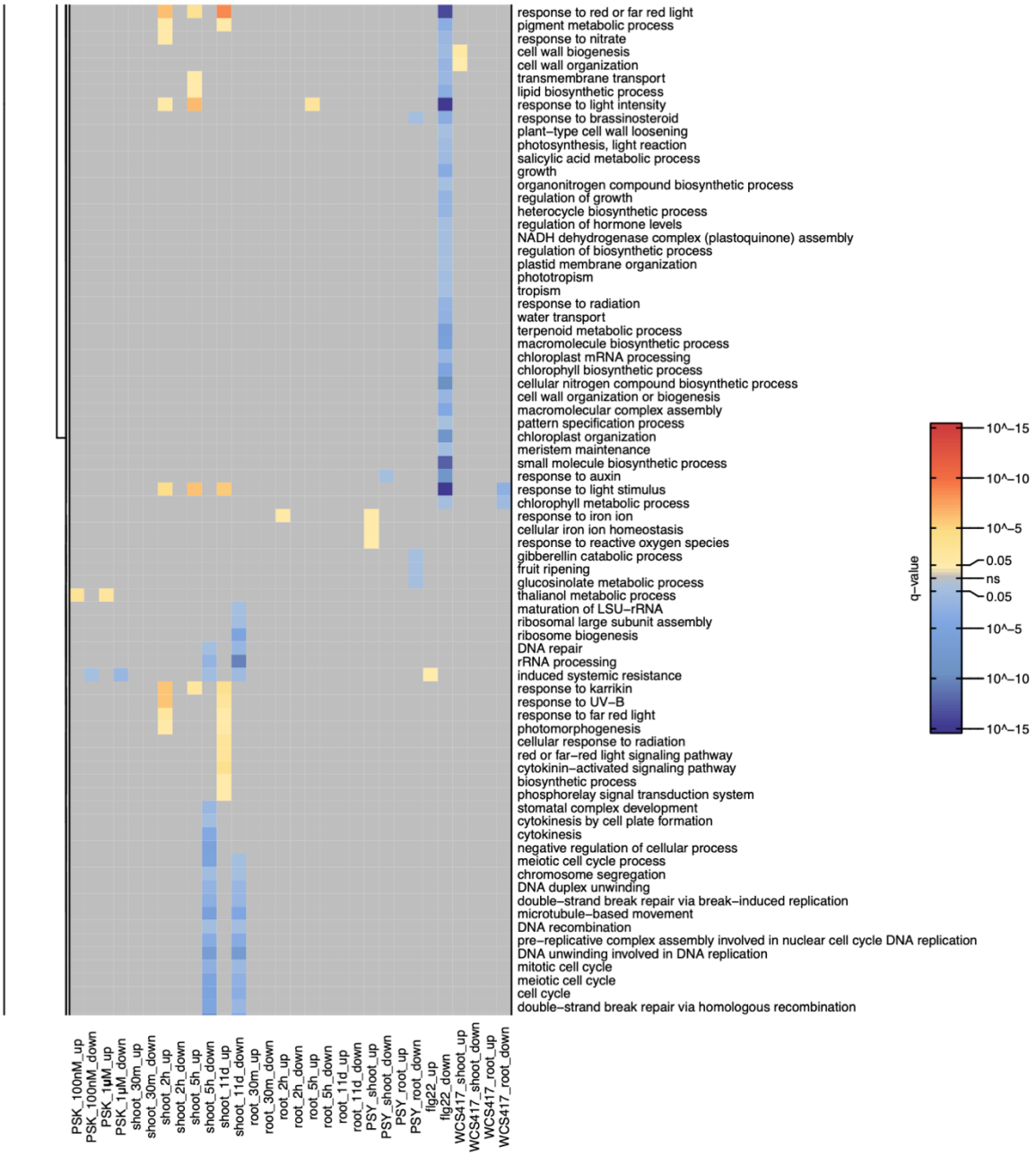

Figure 22. Heatmap of all enriched GO_BP terms, continued

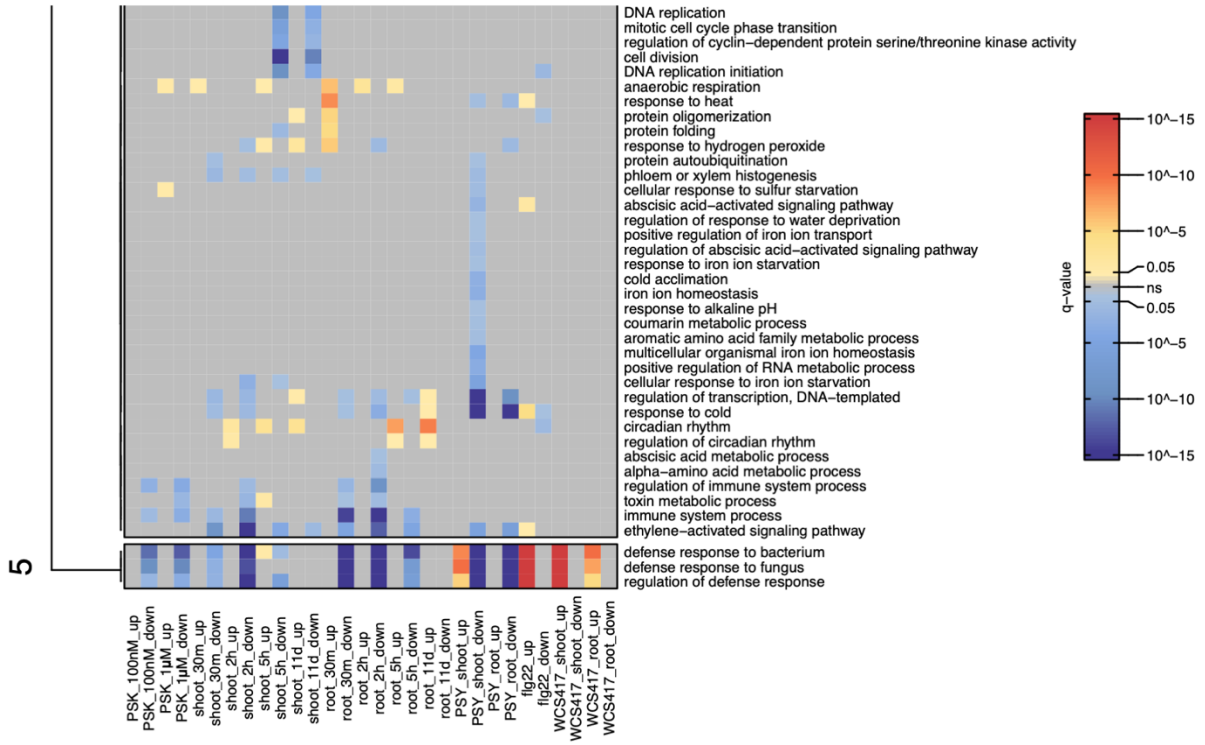

Figure 22. Heatmap of all enriched Gene Ontology Biological Process (GO_BP) terms from PSK, PSY, flg22, and WCS417 treatments. The dendrogram on the side of the heatmap illustrates the hierarchical clustering of row using k-means clustering with numbers on the branches denoting the distance measures. Red denotes functional terms enriched from up-regulated DEGs, while blue denotes functional terms enriched from down-regulated DEGs. The intensity of color reflects their significance measured by q-value, utilizing the cut-off of q-value < 0.05.

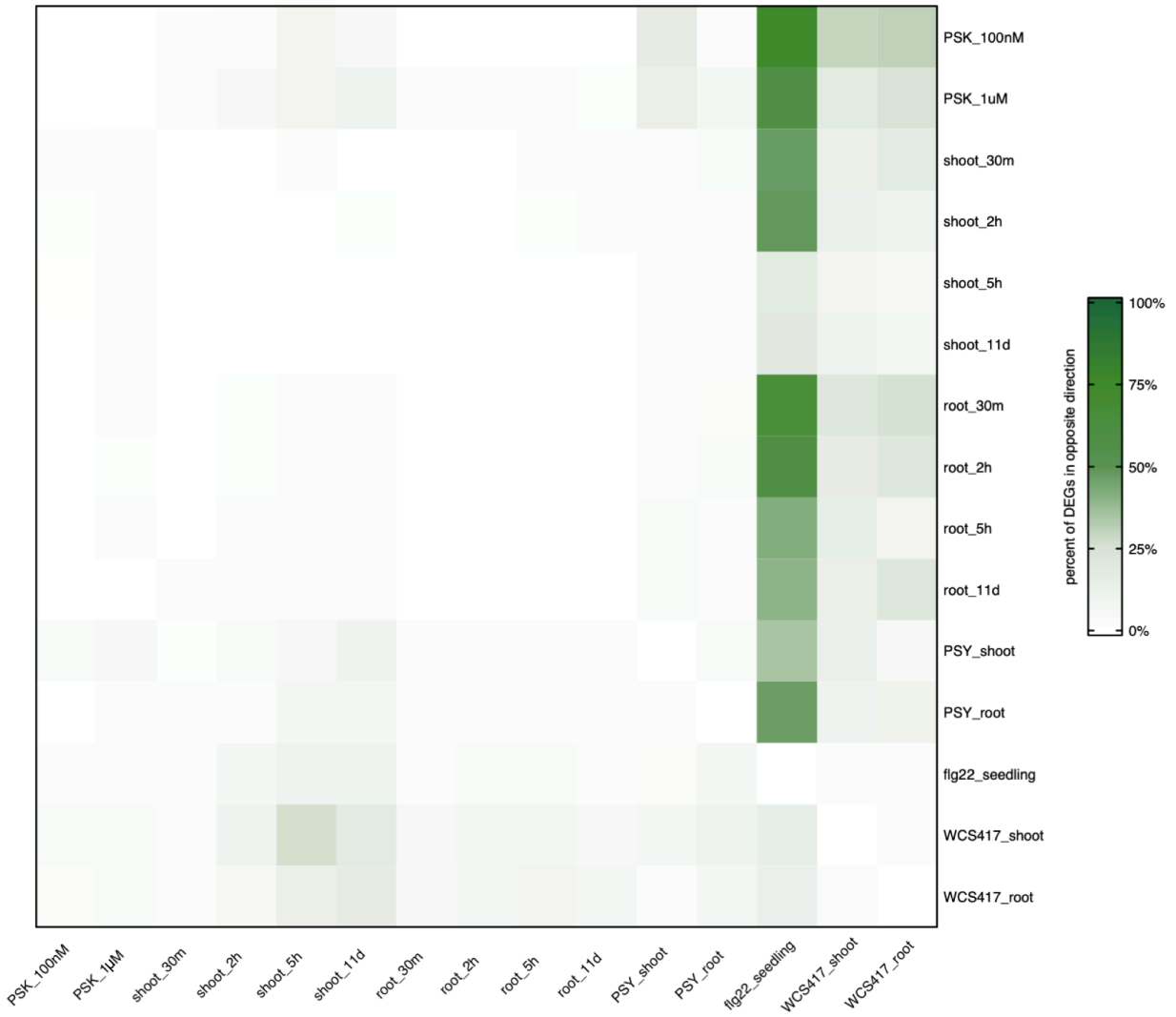

Figure 23. Heatmap of the percentage of DEGs regulated in the opposite direction by PSK, PSY, flg22 and WCS417 among all DEGs, using row category as the base. The intensity of green indicates percentage.

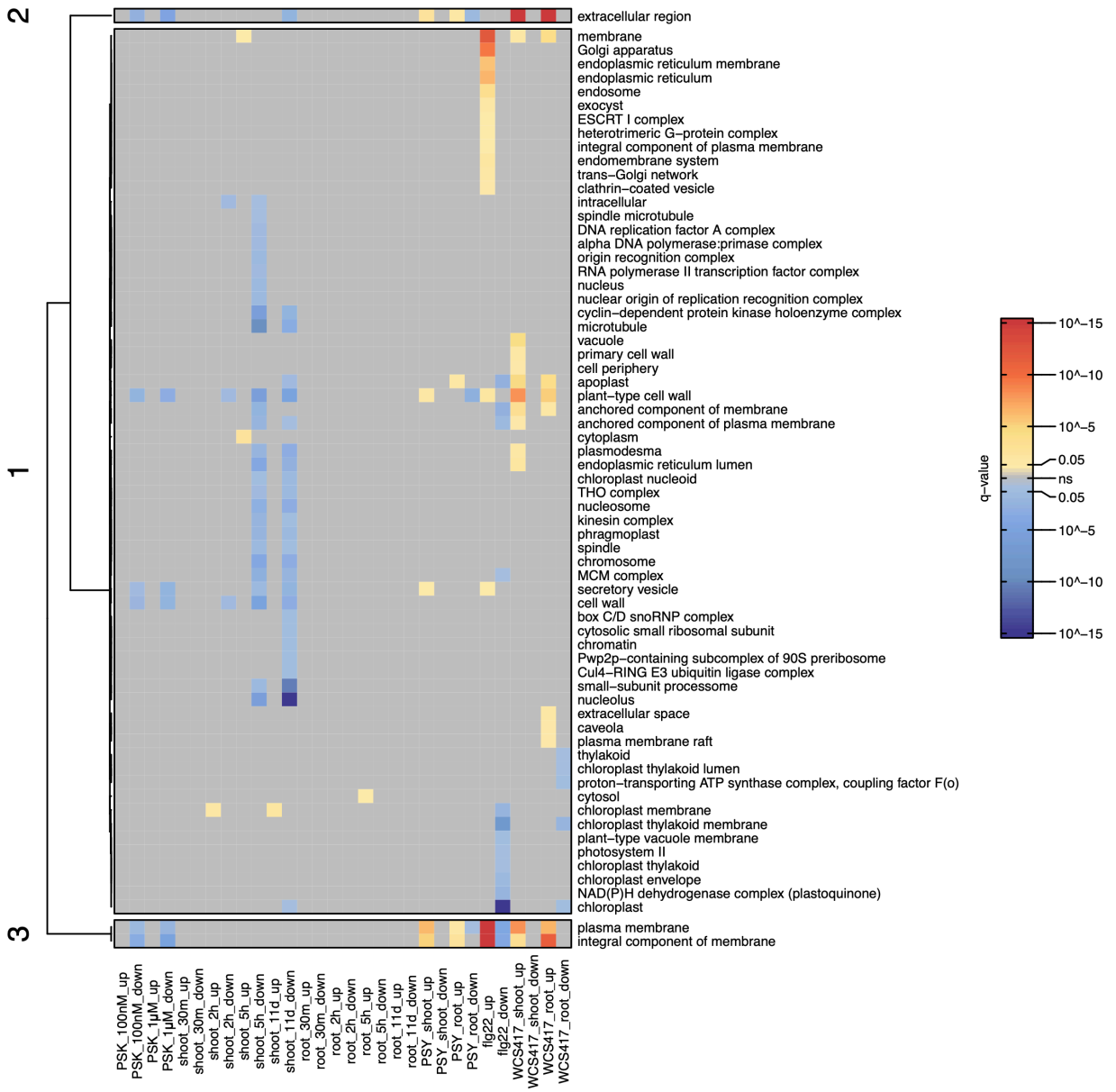

Figure 24. Heatmap of all enriched Gene Ontology Cellular Component (GO_CC) terms from PSK, PSY, flg22, and WCS417 treatments. The dendrogram on the side of the heatmap illustrates the hierarchical clustering of row using k-means clustering with numbers on the branches denoting the distance measures. Red denotes functional terms enriched from up-regulated DEGs, while blue denotes functional terms enriched from down-regulated DEGs. The intensity of color reflects their significance measured by q-value, utilizing the cut-off of q-value < 0.05.

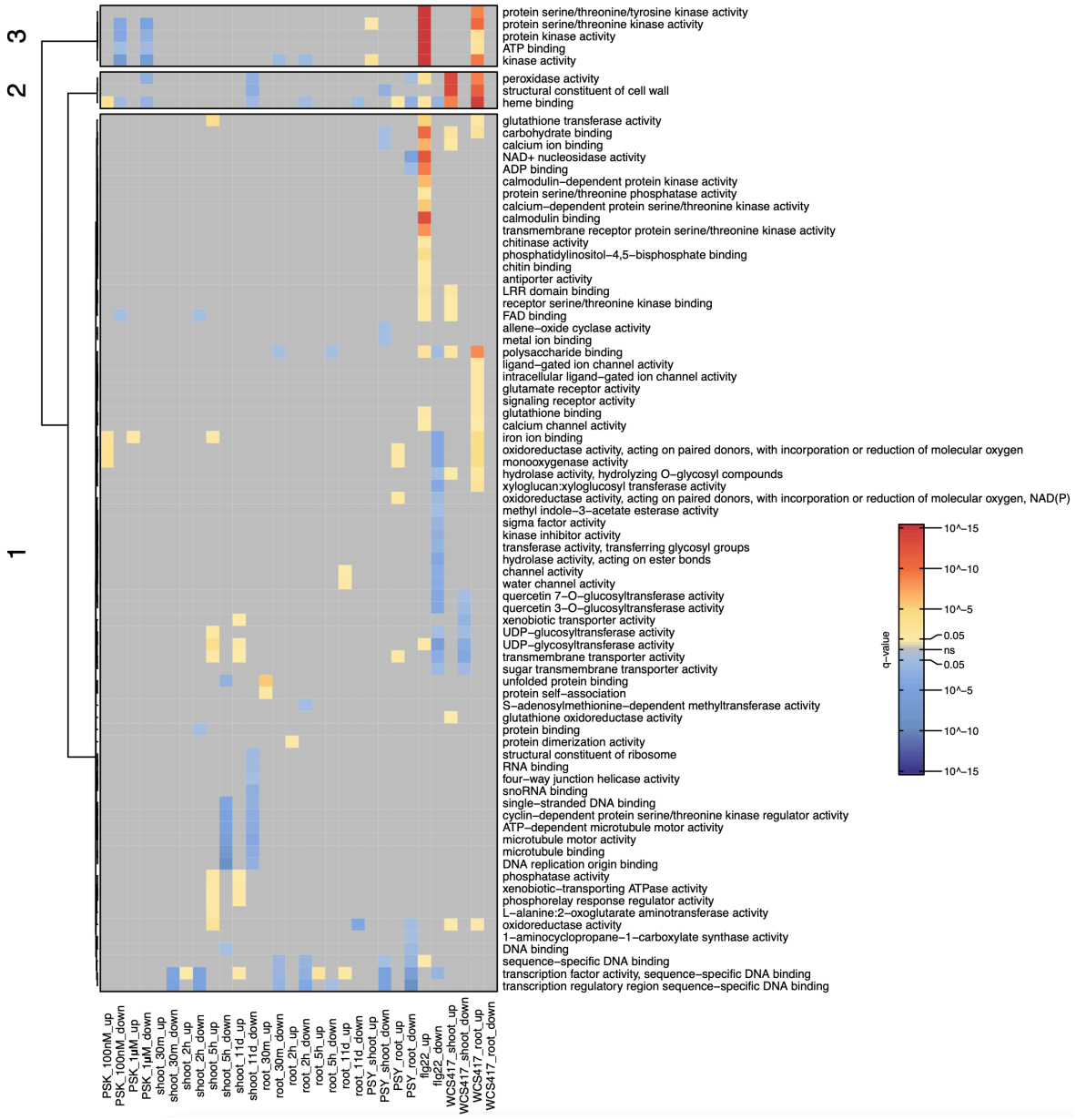

Figure 25. Heatmap of all enriched Gene Ontology Molecular Function (GO_MF) terms from PSK, PSY, flg22, and WCS417 treatments. The dendrogram on the side of the heatmap illustrates the hierarchical clustering of row using k-means clustering with numbers on the branches denoting the distance measures. The dendrogram on the side of the heatmap illustrates the hierarchical clustering of row using k-means clustering with numbers on the branches denoting the distance measures. Red denotes functional terms enriched from up-regulated DEGs, while blue denotes functional terms enriched from down-regulated DEGs. The intensity of color reflects their significance measured by q-value, utilizing the cut-off of q-value < 0.05.

2.7 bZIP TFs comprise another important TF family in PSK signaling pathway

Besides WRKY TFs as the most commonly shared TFs that were enriched from DEGs of PSK, PSY, flg22, and WCS417 treatments, several basic region/leucine zipper motif (bZIP) transcription factors were also common TFs shared by these treatments (Figure 17). However, unlike the regulatory effects of WRKY TFs, these shared bZIP TFs were primarily enriched from PSK up-regulated DEGs and from PSY, flg22, and WCS417 down-regulated DEGs (Figure 26, 27). The bZIP TFs are functionally related to plant biotic and abiotic stresses [39], suggesting PSK signaling is also involved in these plant responses via bZIP TFs but exhibiting a different regulatory pattern from WRKY TFs.

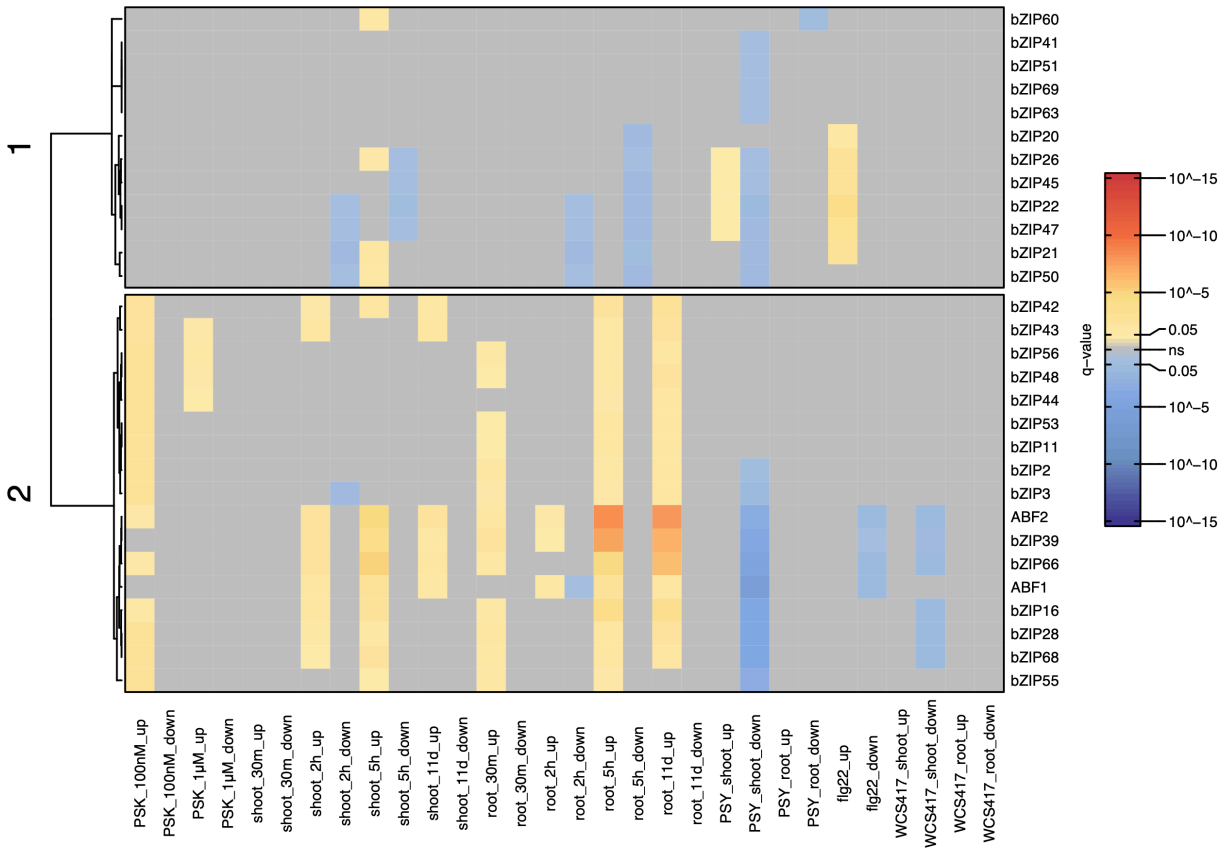

Figure 26. Heatmap of enriched bZIP TFs from PSK, PSY, flg22, and WCS417 up- and down-regulated DEGs. The dendrogram on the side of the heatmap illustrates the hierarchical clustering of row using k-means clustering with numbers on the branches denoting the distance measures. Red denotes enrichment from up-regulated DEGs, while blue denotes enrichment from down-regulated DEGs. The intensity of color reflects their significance measured by q-value, utilizing the cut-off of q-value < 0.05.

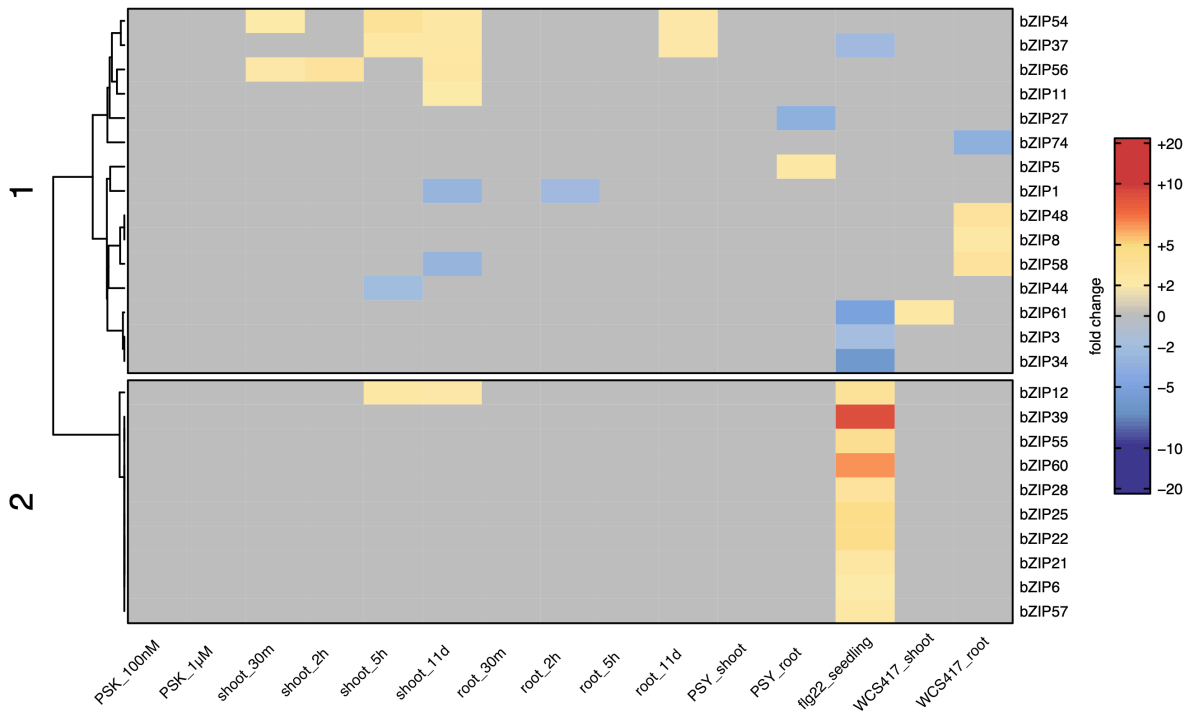

Figure 27. Heatmap of differentially expressed bZIP TFs with PSK, PSY, flg22, and WCS417 treatments. The dendrogram on the side of the heatmap illustrates the hierarchical clustering of row using k-means clustering with numbers on the branches denoting the distance measures. Red indicates up-regulation, while blue indicates down-regulation. The intensity of color reflects their fold changes, utilizing the cut-off of ≥ 2-fold change and adjusted p-value < 0.05.

3 PSK ANTAGONIZES WITH THE PATHOGEN-ASSOCIATED MOLECULAR PATTERN FLG22

ATTRIBUTIONS

This chapter integrated work from Dr. Joanna Jelenska and Dr. Jessica Morgan. Dr. Jelenska performed the MPK phosphorylation and FLS2 quantification measurements, and analyzed reactive oxygen species (ROS) data. Dr. Jessica Morgan performed the ROS experiment. I conducted bioinformatic analysis, performed the callose deposition experiment, integrated data and produced figures.

3.1 PSK and flg22 have opposite regulatory effects on genes

Flagellin 22 (flg22) induces a broad spectrum of plant defense genes and physiological responses [40, 41], whereas our transcriptomic analysis revealed that PSK elicits the opposite effects. A comparison of PSK-induced DEGs with flg22-induced DEGs [31] revealed intriguing patterns (Table 10). In our seedling samples, 86.27% (88 out of 102) of down-regulated DEGs induced by 100 nM PSK were up-regulated by flg22, and 50% (18 out 36) of PSK up-regulated DEGs induced by PSK were down-regulated by flg22 (Figure 28, Table 10). A significant proportion of PSK-induced DEGs - 76.81% (106 out of 136) – overlapped with DEGs induced by flg22, but with opposite directions (Table 10). Across various PSK treatments, ranging from 59.46% to 76.81% of DEGs were oppositely regulated by PSK and flg22 in seedling samples, 18.11% to 48.02% in shoot samples, and 39.53% to 63.75% in root samples (Figure 23). Irrespective of PSK

treatment methods or plant tissue, a considerable number of DEGs consistently exhibit opposite regulatory patterns in response to flg22.

I further compared the differentially expressed *WRKY* TF genes and WRKY TFs enriched from DEGs that may target their downstream genes in PSK and flg22 cases (Figure 20, 21, Table 8, 9). All the 34 WRKY TFs enriched from PSK-induced DEGs were included within the 42 WRKY TFs enriched from flg22-induced DEGs, and these shared WRKY TFs were enriched from PSK down-regulated DEGs and flg22 up-regulated genes (Figure 18). Among the 31 differentially expressed *WRKY* TF genes in PSK-treated plants and 45 differentially expressed *WRKY* TF genes in flg22-treated plants, 28 were found to be the same WRKY TFs. Notably, 24 out of these 28 shared WRKY TFs were regulated by PSK and flg22 in opposite directions (Figure 19).

Overall, from the TF enrichment analysis, the common WRKY TFs were enriched from PSK down-regulated DEGs, while from flg22 up-regulated DEGs. This is further supported by that fact that WRKY TFs were only overrepresented in flg22 up-regulated genes, but not in the down-regulated genes (Table 3, 4, 5). Moreover, PSK primarily down-regulated *WRKY* TF genes, while flg22 up-regulated this similar set of *WRKY* TF genes.

From functional enrichment analysis, the majority of shared Gene Ontology Biological Process terms between PSK and flg22 were related to plant defense. Additionally, PSK down-regulated genes associated with plant defense, whereas flg22 up-regulated gene within these functional terms (Figure 22).

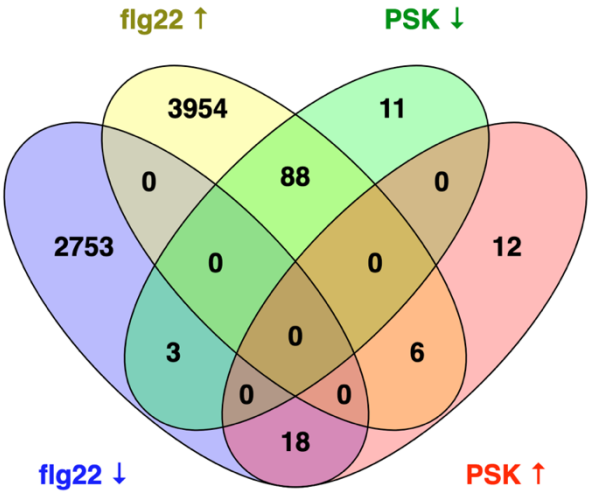

Figure 28. Venn diagram of the number of up- or down-regulated DEGs induced by PSK and flg22.

Category	Number	Total	Percentage
flg22 ↑ PSK ↓	88	102	86.27%
flg22 ↓ PSK ↓	3	102	2.94%
flg22 - PSK ↓	11	102	10.78%
flg22 ↓ PSK ↑	18	36	50.00%
flg22 ↑ PSK ↑	6	36	16.67%
flg22 - PSK ↑	12	36	33.33%
Opposite to flg22	106	138	76.81%
Same as flg22	9	138	6.52%
Not respond to flg22	23	138	16.67%

Table 9. Summary of number of DEGs in each category and their percentages among DEGs induced by PSK. In total of 138 PSK-induced DEGs, 36 were up-regulated and 102 were down-regulated by PSK.

3.2 PSK has no effects on ROS induced by flg22

The common WRKY TFs shared by PSK and flg22 and their opposite regulatory effects on plant defense-related genes suggest a potential counteractive role of PSK against the impact of flg22 on plant defense responses. We tested which signaling steps upstream of gene expression may be targeted by PSK.

One of the very early responses to flg22, the ROS burst [42, 43], was mostly unaffected by PSK (Figure 29, 30).

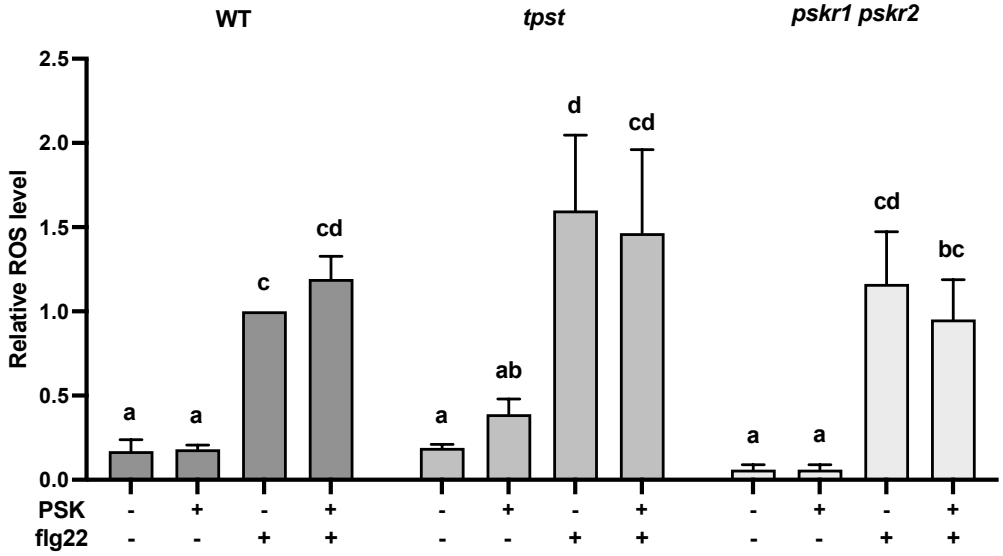

Figure 29. Effect of PSK on flg22-induced ROS burst. PSK pretreatment does not affect flg22-induced ROS. *tpst* plants have higher ROS response than WT (Figure 30). The mean values of relative ROS accumulation from several experiments are shown (see Methods). Different letters indicate significant difference in one-way ANOVA analysis (p-value < 0.05, Fisher's test).

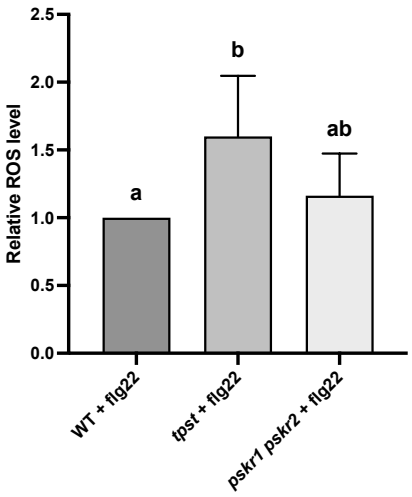

Figure 30. flg22-induced ROS in different genotypes: *tpst* plants have a higher ROS response than WT. Different letters indicate significant difference in one-way ANOVA analysis (p-value < 0.05, Fisher's test).

3.3 PSK attenuates MPK phosphorylation

Another early response to flg22, MAP kinase phosphorylation, is upstream of defense gene expression activation [30, 43]. All genotypes tested (WT, *tpst* and *pskr1 pskr2*) showed flg22-induced phosphorylation of MAP kinases, although the absolute induction was higher in *tpst* and lower in *pskr1 pskr2* relative to WT (Figure 31, 32). When pretreated with PSK, there was modest attenuation of flg22-induced phosphorylation (Figure 31), while the basal level of MPK3 was unaffected (Figure 33, 34). These effects on phosphorylation were receptor-dependent (see *pskr1 pskr2* response in Figure 31) . MPK3/6, as established by previous studies, directly interact with WRKY33 and WRKY18/40/60 [44, 45]. This connects MAP kinase phosphorylation and the signaling pathways mediated by WRKY TFs.

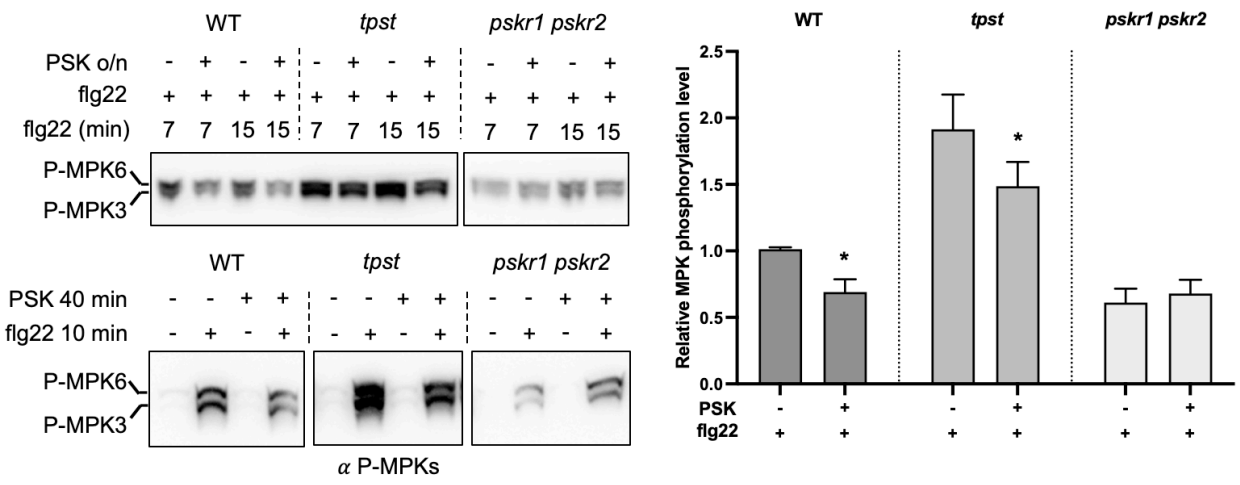

Figure 31. Effect of PSK on flg22-induced MPK phosphorylation. Immunoblots show phospho-MPK3 and -MPK6 in seedlings pretreated overnight with PSK and subsequently induced by flg22 for 7 and 15 min (upper blot, 200 nM peptides) and in seedlings treated for 40 min with PSK and 10 min with flg22 (lower blot, 1 μM peptides). Mock treatment was growth medium with water added instead of peptide(s). In both panels samples are from two gels run, blotted and exposed together. PSK pretreatment reduced flg22-induced MPK phosphorylation. *tpst* plants showed higher MPK phosphorylation than WT and *pskr1 pskr2* (Figure 32). MPK3 and MPK6 were not phosphorylated without flg22 induction. Graph shows mean MPK phosphorylation from several experiments relative to WT with flg22 treatment only. Asterisk indicates ANOVA/Fisher (for pairs) p-value < 0.05, n = 5 (3 for *tpst*).

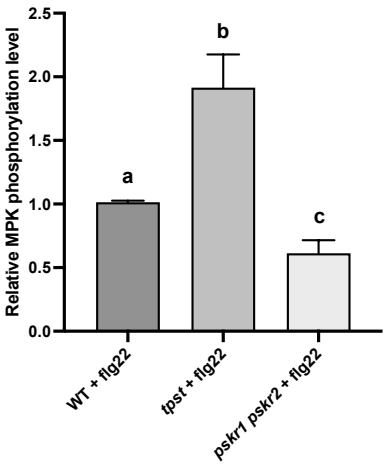

Figure 32. flg22-induced MPK3 and MPK6 phosphorylation in different genotypes. The three genotypes shown have different levels of MPK phosphorylation in response to flg22. Different letters indicate significant difference in one-way ANOVA analysis (p-value < 0.05, Fisher's test).

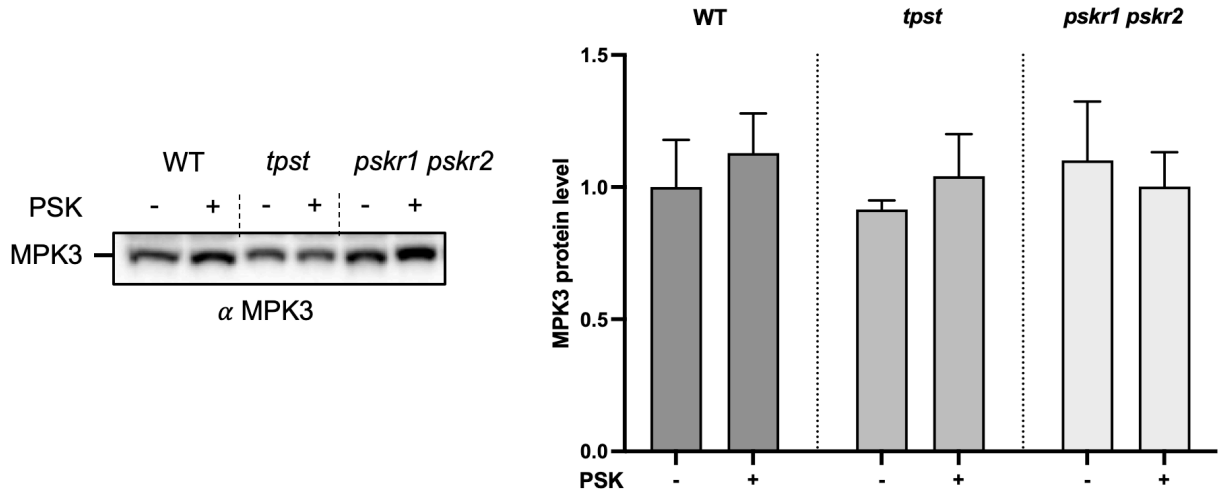

Figure 33. PSK pretreatment does not affect MPK3 protein level. Upper panel, immunoblot with MPK3 antibody of plant samples treated overnight with 1 μM PSK. Graph, mean MPK3 protein level relative to WT without PSK treatment. p-value > 0.05, two-way ANOVA/Fisher or t-test, n = 4 (3 for *tpst*). See also Figure 34.

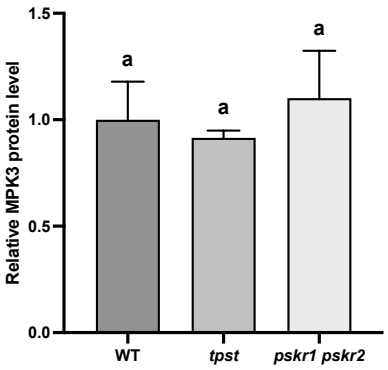

Figure 34. Relative MPK3 protein level was similar in all genotypes. Different letters indicate significant difference in one-way ANOVA analysis (p-value < 0.05, Fisher's test).

3.4 PSK induces a slight increase in FLS2 protein accumulation

Suppression of PAMP responses may result from altered receptor levels, therefore we tested levels of flg22 receptor FLS2 after PSK treatment. Surprisingly, we found that the FLS2 receptor was slightly more abundant in tissues treated with PSK (Figure 35, 36). PSK can attenuate ubiquitination and degradation of its own receptor PSKR1 [46]. It is plausible that PSK stabilizes other receptors such as FLS2 and prevents their endocytosis, which is crucial for FLS2 signaling [47-49]. *tpst* plants were more sensitive to flg22 treatment, as they showed higher ROS burst and MPK phosphorylation, and had higher level of FLS2 protein than wild-type plants (Figure 30, 32, 34).

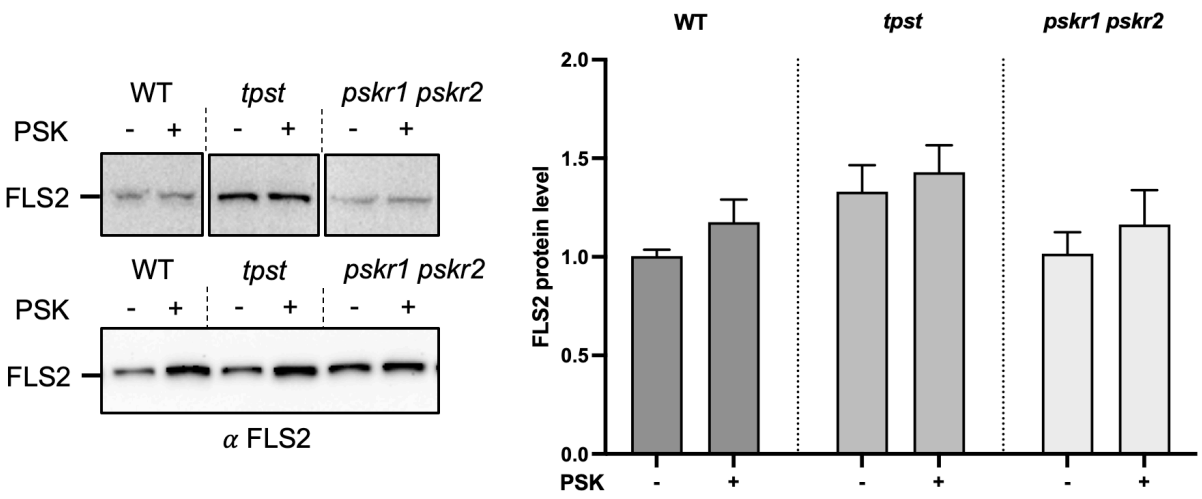

Figure 35. PSK treatment does not significantly change FLS2 protein level. The immunoblots show FLS2 protein in seedlings treated overnight with 200 nM flg22. All samples are from the same gel/blot. In some experiments PSK treatment increased FLS2 levels in WT and *tpst* plants (lower immunoblot), however analysis of all data rendered the difference not significant (graph). p-value > 0.05, two-way ANOVA/Fisher or t-test, n = 14 (10 for *tpst*). FLS2 protein was analyzed in the same experiments as MPK phosphorylation and basal level.

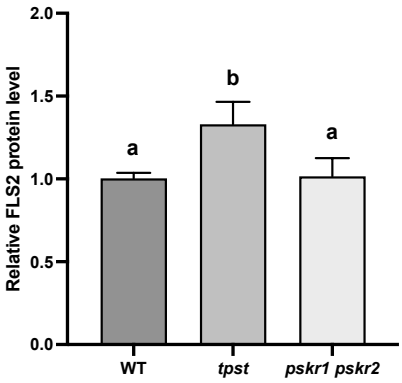

Figure 36. FLS2 levels were higher in *tpst* than WT and *pskr1 pskr2* plants. Different letters indicate significant difference in one-way ANOVA analysis (p-value < 0.05, Fisher's test).

3.5 PSK reduces flg22-induced callose deposition

I further examined flg22-induced callose deposition, which is a late response to flg22 [50]. Prior to treating WT, *tpst*, *pskr1 pskr2* plant seedlings with 1 μM flg22 or mock treatments of water for 24 hours on day 8, I implemented a 24-hour pretreatment on day 7 with 100 nM PSK or mock treatments of water. The density of flg22-induced callose deposits was significantly reduced by PSK pretreatment in WT and *tpst* plants, but not in *pskr1 pskr2* plants, indicating a PSKR-dependent suppression by PSK (Figure 37, 38). The relative area of callose deposition also displayed this PSK- and PSKR-dependent trend, while the average size of callose deposits remained similar across the three genotypes (Figure 39, 40).

Taken together, PSK pretreatment reduces the number of flg22-induced callose deposits only in the presence of PSKRs, with no significant effects on callose deposit sizes. A possible molecular explanation at the gene expression level for this effect is through regulation of the *ATL31* gene that positively contributes to callose deposition [51]. *ATL31* was down-regulated by PSK, but up-regulated by flg22 (Figure 11).

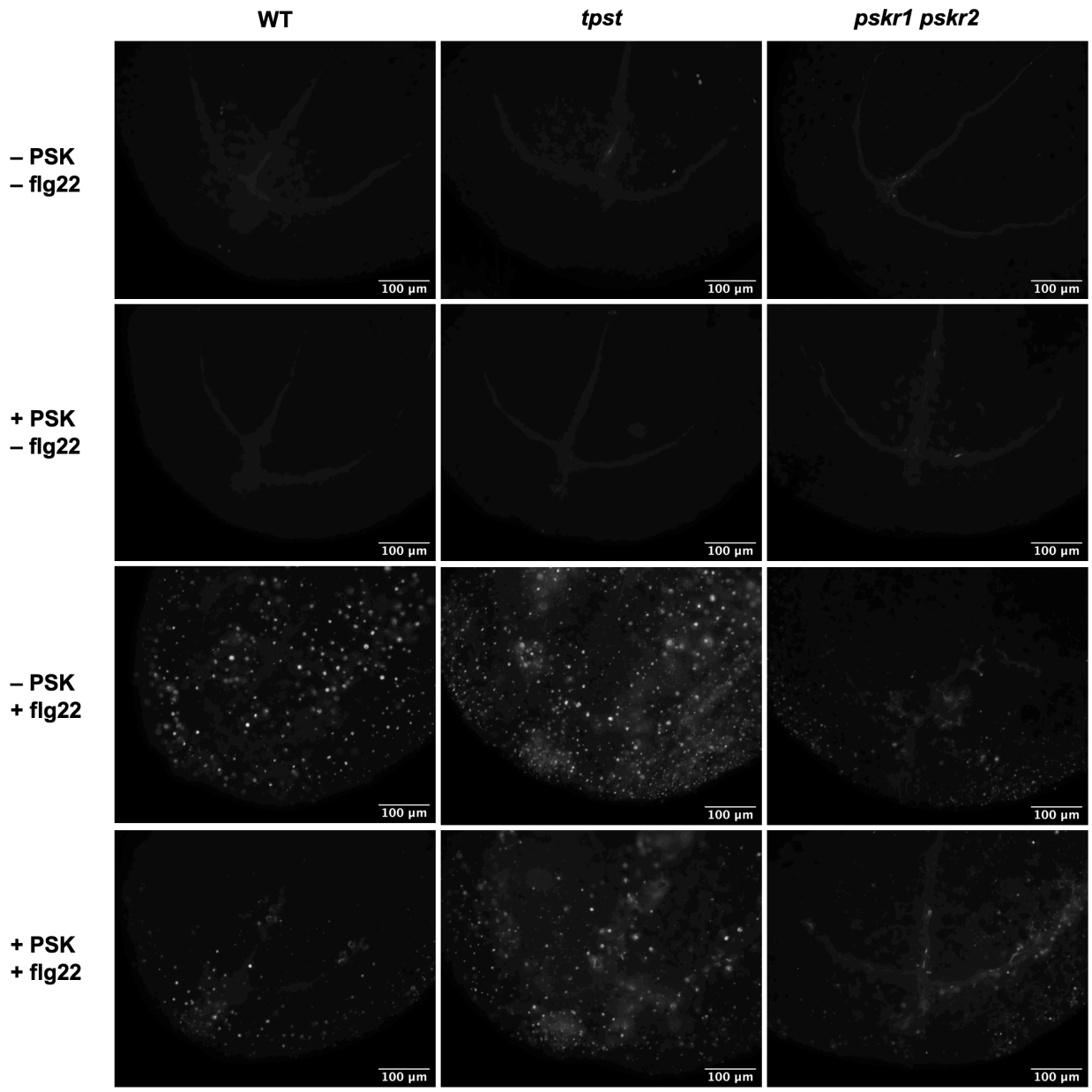

Figure 37. Callose deposition visualized by aniline blue staining and fluorescence microscopy in WT, *tpst*, *pskr1 pskr2* plants treated with or without PSK and flg22.

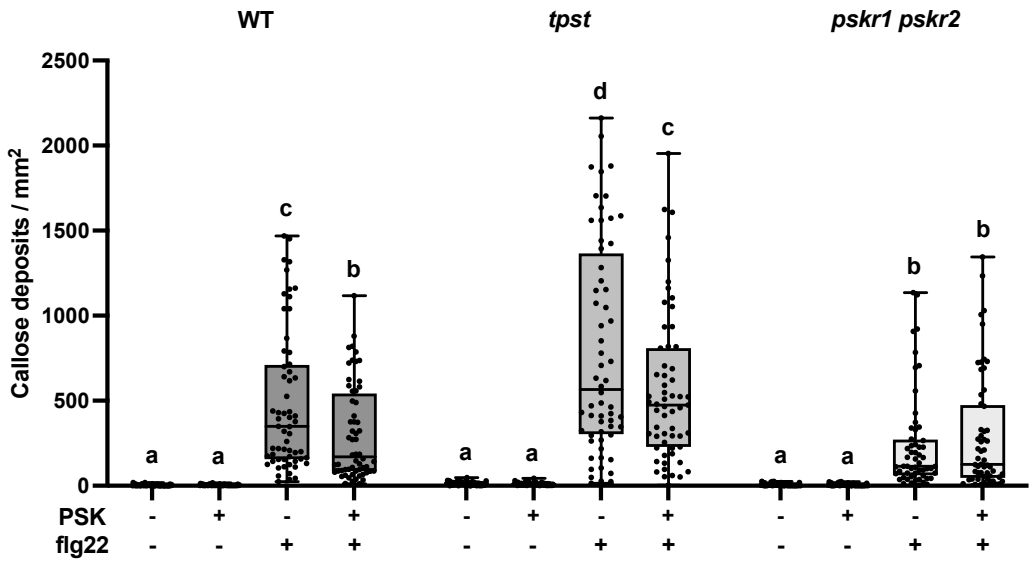

Figure 38. Callose density quantified by the number of callose deposits per mm^2 in WT, *tpst*, *pskr1 pskr2* plants treated with or without PSK and flg22 (each treatment group contains 30 seedlings with 60 cotyledons). Different letters indicate significant difference in one-way ANOVA analysis (p-value < 0.05, Tukey's test).

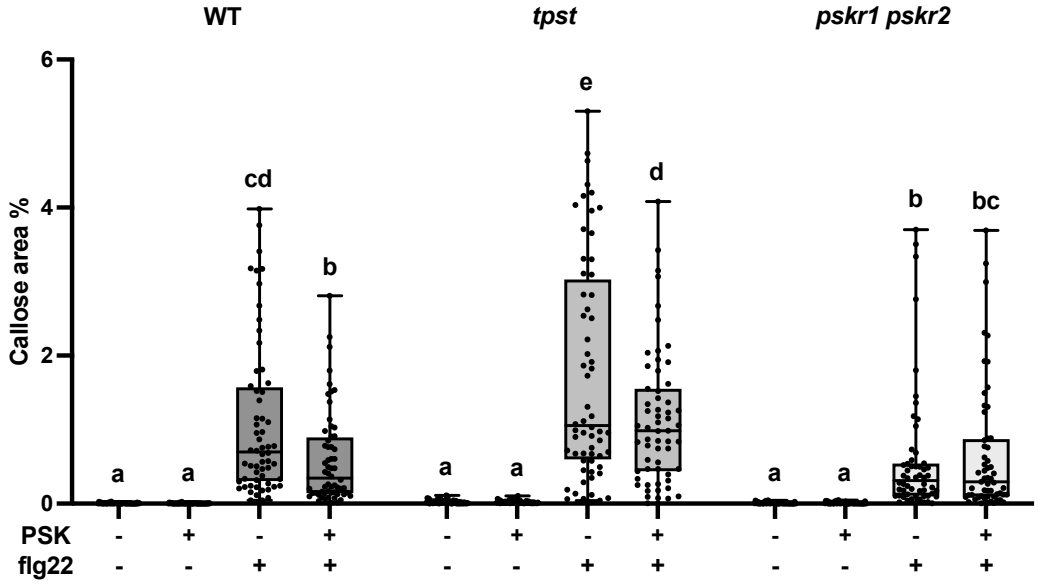

Figure 39. Callose area percentage calculated as the area of callose deposits relative to the total plant area in WT, *tpst*, *pskr1 pskr2* plants treated with or without PSK and flg22 (each treatment group contains 30 seedlings with 60 cotyledons). Different letters indicate significant difference in one-way ANOVA analysis (p-value < 0.05, Tukey's test).

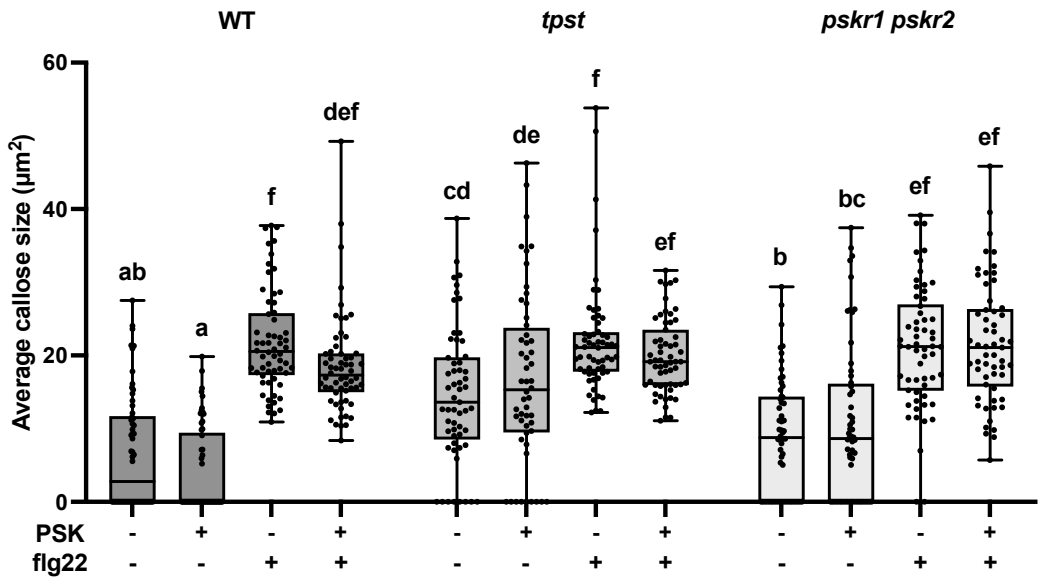

Figure 40. The average size of callose deposits in WT, *tpst*, *pskr1 pskr2* plants treated with or without PSK and flg22 (each treatment group contains 30 seedlings with 60 cotyledons). Different letters indicate significant difference in one-way ANOVA analysis (p-value < 0.05, Tukey's test).

4 DISCUSSION

In this study, I conducted a comprehensive transcriptional profiling of Arabidopsis responses to PSK and uncovered PSK's role in mediating the trade-off between plant growth and defense. WRKY transcription factors were over-represented among the transcription factors regulating PSK-responsive genes. Furthermore, these WRKY transcription factors are common to those involved in the response to the pathogen-associated molecular pattern flg22, a PAMP derived from bacterial flagellin, but were regulated in opposite directions. PSK is capable of attenuating flg22-induced MPK phosphorylation and callose deposition. Moreover, WRKY TFs are the common TFs shared by PSK and PSY with primarily down-regulation effects, while flg22 and WCS417 with predominantly up-regulation effects.

4.1 PSK's role in mediating plant growth-defense trade-off

Previously, it was established that PSK generally promotes plant growth while attenuating plant defense mechanisms in some cases, and PSKR1 plays an important role in mediating the trade-off between plant growth and defense in the rhizosphere microbiome [21-24]. My transcriptomic analysis offers novel insights into PSK's influence on tipping the balance of plant growth-defense trade-off. The suppression effect of PSK on defense-related genes is more predominant in the transcriptomics than its activation effect on growth-related genes. Considering that significantly fewer genes and functional terms are linked with growth promotion compared to defense suppression, it is plausible that some of PSK's growth-promoting effects may stem from the down-regulation of plant defense responses. The defense-suppression effect conserves energy

and diminishes non-essential defense activities to prioritize plant growth, especially during the early development stage of Arabidopsis.

4.2 PSK's effects on ROS, FLS2 and flg22-induced responses

PSK treatment did not reduce FLS2 protein levels and even slightly increased them. Similarly, an early response to flg22, the ROS burst mediated by plasma membrane RBOHD [52], was mostly unaffected by PSK treatment. However, other branches of the flg22 immune response, MAP kinase phosphorylation (which indicates MAP kinase activation) and callose deposition, were reduced by PSK treatment despite the trend of FLS2 receptor level to become elevated. Differential effects on immune response branches are not uncommon and may reflect different subcellular location of signaling FLS2 pools [49, 53].

The MAP kinase cascade directly activates WRKY TFs in plant immune signaling in response to PAMPs [30, 43]. Reduced phosphorylation of MPK3 and MPK6 supports my transcriptomics analysis, which shows opposite regulation of WRKY family transcription factors by PSK and flg22. Despite different effects on distinct branches of immune signaling, PSK is predicted to interfere with transcriptional reprograming in response to flg22, since we found reduced MPK phosphorylation and attenuated callose deposition in response to flg22. This is in turn may permit the greater allocation of resources to growth versus defense.

PSK possesses the ability to diminish flg22-induced callose deposition, resulting in longer-term consequences. However, PSK does not significantly reduce the expression levels of *PMR4*, the pathogen-induced specific callose synthase (Figure 11). This is consistent with previous finding that the gene expression levels of callose synthase family genes are only moderately changed in response to various stresses [54]. Therefore, the reduced callose deposition after PSK

treatments was not due to a down-regulation of the callose synthase gene *PMR4*. Instead, PSK down-regulates the expression of *ATL31*, a membrane-associated ubiquitin ligase that involved in plant defense-induced callose deposition [55]. *ATL31* is up-regulated in response to flg22 (Figure 11), and its over-expression enhances callose deposition [51]. PSK may counteract with flg22's effect on *ATL31* that promotes callose deposition. Additionally, PSK down-regulates genes associated with salicylic acid and abscisic acid (Figure 11), which positively contribute to callose deposition [56]. This downregulation may constitute an indirect additional mechanism to reduce callose deposition.

An unexpected finding was that FLS2 protein levels were higher in the *tpst* plants than WT (Col-0) (Figure 36). This may explain why ROS, MPK phosphorylation and callose levels in response to flg22 in *tpst* plants were higher than in other genotypes tested (Figure 30, 32, 38). FLS2 protein levels and flg22-induced ROS were similar in *pskr1 pskr2* and WT plants, where MAP kinase phosphorylation was lower in *pskr1 pskr2* (Figure 30, 32, 36). Thus, it seems unlikely that loss of PSK signaling can explain FLS2 protein levels in *tpst* plants. Rather, a different TPST substrate peptide may repress basal FLS2 levels.

4.3 The mechanism of PSK's antagonism with flg22

PSK antagonizes the effects of flg22 at multiple different levels (Figure 41). The inhibitory effect of PSK on flg22-induced MPK3/6 phosphorylation manifests rapidly, within 7 to 15 minutes (Figure 31). Previous studies demonstrated that MPK3/6 phosphorylates WRKY33, WRKY40 [44, 45]. I found that PSK down-regulates WRKY33 and WRKY40 expression while flg22 up-regulates them, indicating opposite regulatory directions (Figure 19). Furthermore, 48 WRKY TFs were identified to be the substrates of MPK phosphorylation *in vitro* [57]. Our analysis reveals that

PSK and flg22 both target a large and similar set of WRKY TFs, yet they exert opposite regulatory effects on these *WRKY* TF genes and downstream defense genes (Figure 17, 18). The transcriptional changes were evident within the time frame of 30 minutes to 5 hours. Additionally, PSK reduces flg22-induced callose deposition. This was validated over a longer duration of 24 to 48 hours (Figure 37, 38).

Taken together, PSK attenuates various of flg22-induced effects, including MPK phosphorylation, *WRKY* TF genes and defense genes expression, and callose deposition. These effects were observable within a short span of 7 minutes to a longer duration of 48 hours. Notably, both the PSK receptor PSKR1 and flg22 receptor FLS2 bind to the co-receptor kinase BAK1 [58, 59]. Although it is possible that a competition mechanism at the receptor level exists (Figure 9), the very early ROS response is unaffected.

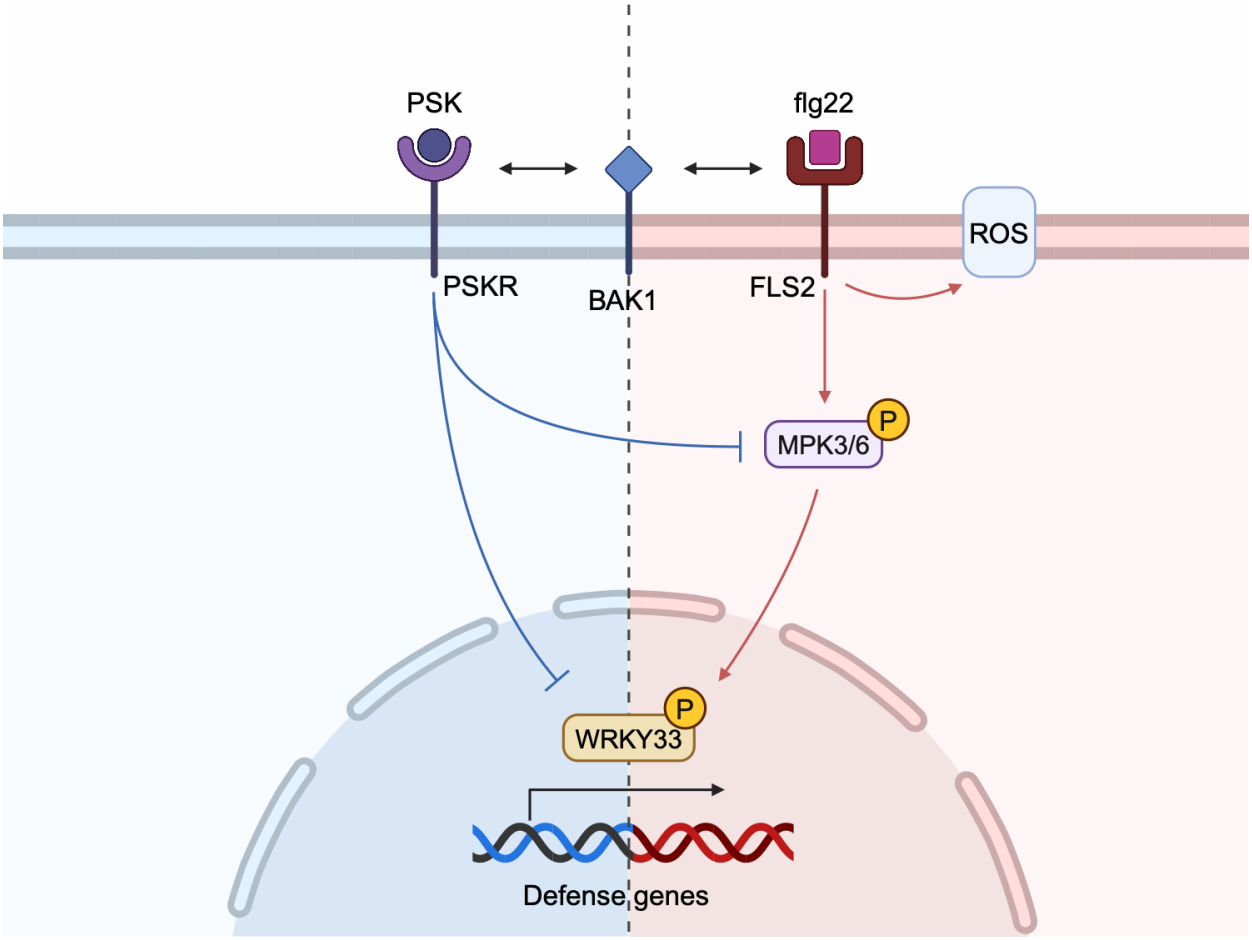

Figure 41. Model of PSK and flg22 antagonism. PSKR competes with FLS2 for binding to BAK1. PSK reduces the phosphorylation level of MPK3/6, and down-regulates the expression level of WRKY33 and many defense genes. These effects are opposite to flg22's effects. However, PSK does not affect ROS level.

4.4 The effects of PSK, PSY, flg22, and WCS417 are different despite similar sets of WRKY TFs and overlapping regulated genes

In terms of their regulatory effects on WRKY TFs and plant defense-related genes, the TPST-sulfated PSK and PSY peptides induce changes that are more similar when compared with the effects of flg22 and WCS417 bacterium. This alignment is consistent with the number of differentially expressed genes (DEGs) in opposite directions (Figure 23). However, PSK diverges

from PSY in its effects on genes associated with protein phosphorylation, kinase activity, and cellular positioning within the plasma membrane (Figure 22). PSY's effects are more similar to those of flg22 and WCS417 than to PSK in these functional terms. This suggests that unknown mechanisms may underlie the signaling perception and activation processes of PSK and PSY. One example is the pattern-triggered immunity marker gene *FRK1*. PSK down-regulates *FRK1* expression, while PSY, flg22 and WCS417 all up-regulate its expression (Figure 16). Moreover, concerning genes associated with GO_BP term "plant epidermis development", PSK, PSY, and WCS417 all up-regulate these genes, whereas flg22 down-regulates them. This pattern aligns with the positive effects of PSK, PSY, and WCS417 on plant growth and the highly inhibiting effects of flg22 [36-38].

5 CONCLUSIONS

PSK is a peptide hormone that demonstrates the capacity to promote plant growth and regulates plant defense. Its potential in bioenergetics, particularly in enhancing plant biomass and increasing disease resistance, is substantial. However, a thorough understanding of the direct transcriptional responses triggered by PSK in plants is still lacking. In order to bridge this gap of knowledge, I conducted a comprehensive transcriptional profiling of plants treated with synthetic PSK to identify genes regulated by PSK.

In this study, I utilized *tpst* plants, which are unable to produce native active sulfated PSK, to eliminate the influence of endogenous PSK. *tpst* plants exhibited significant shorter root lengths compared to wild-type plants. Application of exogenous PSK promotes root growth of *tpst* plants in a PSK receptors-dependent manner, while non-sulfated PSK elicits no such effect on root growth. To ensure precise control over the concentration and duration of PSK treatment, I grew plants hydroponically and confirmed the above phenotypes were consistent with plants grown in agar plates and soil. The root growth promotion effect mediated by PSK was found to be dependent on the concentration and duration of PSK treatment, allowing for the exploration of PSK's dose effect and a time-series analysis.

The transcriptional profiling consisted of two sets of RNA-seq experiment. One was 7-day-old *tpst* plants treated with 100 nM and 1 μM PSK respectively to investigate the dose effects of PSK and profiled at the whole seedling level. The other was 11-day-old *tpst* plants treated with 10 nM PSK for 30 minutes, 2 hours, 5 hours and 11 days to discern duration effects of PSK treatment and profiled as shoot and root separately to reveal tissue-specific response. By integrating the

diverse treatment settings and comparing transcriptional readouts, I was able to identify the core PSK responses that are irrespective of plant age, tissue type, PSK concentration and exposure duration.

Interestingly, from differential expression analysis and functional enrichment analysis, I did observe some growth-related genes were up-regulated by PSK. However, PSK's down-regulation effect on defense-associated genes were more pronounced and significant in plant transcriptomics. To elucidate the TFs involved in regulating PSK-responsive genes, I conducted TF enrichment analysis of those DEGs and found that a specific TF family, WRKY TFs, accounted for a significant portion and were over-represented within all the TFs enriched. WRKY TFs are associated with plant defense, thus shedding light on the underlying connection.

Furthermore, I integrated published data of another TPST-sulfated growth-promoting peptide PSY, a root growth-promoting beneficial bacterial WCS417, and a pathogen-associated molecular pattern flg22, to investigate if overlapping transcription factors and targeting genes were involved. The results indicated that WRKY TFs emerged as a common TF family shared by PSK, PSY, flg22 and WCS417. Genes associated with plant defense were also overlapped in these four treatments. PSK and PSY exhibited more similarity, both down-regulating plant defense response, with WRKY TFs enriched from down-regulated DEGs. flg22 and WCS417 were contrary to PSK's effects, both up-regulating plant defense response, with WRKY TFs enriched from up-regulated DEGs. In fact, a similar set of WRKY TFs and downstream genes were shared by the four distinctive pathways.

Moreover, we examined the contrary effects mediated by PSK and flg22. PSK is capable of attenuating flg22-induced MPK phosphorylation and callose deposition, with opposite effects on WRKY TFs and downstream genes, exhibiting an antagonistic relationship. These

physiological experiments validated my predictions from transcriptional profiling, strengthening the significance of the comparative bioinformatic analysis of PSK and flg22.

In summary, this study revealed novel signaling outputs of plant response to PSK. It highlighted the crucial involvement of WRKY TFs in the PSK signaling pathway and underscored PSK's prominent suppression effect on plant defense at transcriptomic level. While much remains to be explored in the PSK signaling pathway, my research has provided a solid foundation of knowledge regarding the comprehensive gene regulations mediated by PSK. Future experiments building upon this transcriptional profiling could offer further insights, and exploring PSK's interactions with other biological pathways could provide new perspectives on the dynamics of plant regulatory networks.

6 METHODS

6.1 Plant materials and growth conditions

In all experiments, *Arabidopsis thaliana* Columbia-0 (Col-0) ecotype and mutants in the Col-0 background were used. T-DNA insertion mutants *tpst* (SALK_009847), *pskr1* (SALK_008585), *pskr2* (SALK_024464), double mutant *pskr1 pskr2* and transgenic *35S::PSKR1-GFP* line were obtained from Dr. Margret Sauter's group.

Seeds were sterilized with 75% ethanol for 1 min and 5% sodium hypochlorite with 0.05% Tween-20 for 5 min. After sterilization, the seeds were washed with distilled water for five times before being placed on agar plates or in 6-well cell culture dishes for growth. The agar plates were prepared with 35 ml 1/2 Murashige and Skoog (MS) basal medium with 0.05% MES, 1% sucrose, 0.1% MS vitamin solution, and 0.7% agar (pH 5.7). The dishes were supplemented with 5 ml liquid 1/2 MS basal medium with 0.05% MES, 1% sucrose, and 0.1% MS vitamin solution (pH 5.7) per well. The agar plates were positioned vertically and the dishes were placed horizontally in the growth room with 22°C 16 h light / 8 h dark long-day condition (light intensity at 3000 lux). For ROS assays plants were grown in soil for 4 weeks at 20°C with 12 h light / 12 h dark cycle.

6.2 Plant phenotypes and microscope imaging

Images of plants grown on agar plates and in 6-well cell culture dishes were captured using an Epson Perfection V600 Photo Scanner. Images of plants grown in soil were photographed using a Sony Alpha ILCE-7 with 28-70mm Lens. The fluorescence of *35S::PSKR1-GFP* plants was

imaged using a Zeiss LSM 800 Confocal Laser Scanning Microscope with a 40x objective. The fluorescence of callose deposits was imaged using a Leica DMR Microscope with a 10x objective.

6.3 Synthetic peptides

PSK and nsPSK were synthesize by Synbio Technologies, and the lyophilized peptides were dissolved in water and stored at -80°C as 2.3 mM and 2.9 mM stock solutions, respectively. flg22 was synthesized by Biomatik, and the lyophilized peptide was dissolved in water and stored at -80°C as 100 μM stock solutions.

6.4 PSK treatments and RNA extractions

For plant phenotype experiments, PSK treatment was conducted by supplementing medium of agar plates or 6-well cell culture dishes with specific concentrations of PSK. For RNA-seq experiments, three independent biological replicates were used in RNA extraction and RNA-seq. PSK treatment was conducted by adding PSK solution to the growth medium to achieve a final PSK concentration of 100 nM or 1 μM for 5 hours in whole-seedling profiling, or by replacing the growth medium with new medium containing 10 nM PSK for 30 minutes, 2 hours, 5 hours, or 11 days in tissue-specific profiling. Total RNA was extracted from 30 seedlings per replicate at day 7 in whole-seedling profiling, or from 18 seedlings with shoot and root separated at day 11 in tissue-specific profiling, using RNeasy Plant Mini Kit (Qiagen) and the RNase-Free DNase Set for on-column DNase digestion (Qiagen).

6.5 RNA-seq experiments and data analysis

Purified RNA samples were sent to Novogene for poly(A) enrichment mRNA library preparation and sequencing. 20 million 150-bp paired-end reads per sample were generated with the Illumina NoveSeq 6000 System. The obtained reads were mapped to *Arabidopsis thaliana* TAIR10 genome release (ensemblplants_arabidopsis_thaliana_tair10_gca_000001735_1) [60] using HISAT2 (v2.0.5) [61]. FeatureCounts (v1.5.0-p3) was used to count the read numbers mapped of each gene and FPKM (the expected number of Fragments Per Kilobase of transcript sequence per Millions base pairs sequenced) was used to quantify and estimate gene expression [62].

The differential expression analysis was performed with the R package DESeq2 (v1.20.0) [63]. The functional enrichment analysis was conducted at the DAVID Knowledgebase (https://david.ncifcrf.gov/) that integrates Gene Ontology Biological Process (GO_BP), Gene Ontology Cellular Component (GO_CC) and Gene Ontology Molecular Function (GO_MF) databases [64]. The TF enrichment analysis was carried out at PlantRegMap (http://plantregmap.gao-lab.org/) using the FunTFBS method [32]. The heatmaps were generated using the R package ComplexHeatmap (v2.13.1) with rows split by k-means clustering and distance measured by pre-defined Pearson method [65]. The Venn diagrams were created with Venny 2.1.0 [66]. Figure 1, 14, and 41 were created with BioRender.com.

6.6 RNA-seq data accession numbers

The data discussed in this publication have been deposited in NCBI's Gene Expression Omnibus database and are accessible through GEO Series accession number GSE254988 (https://www.ncbi.nlm.nih.gov/geo/query/acc.cgi?&acc=GSE254988).

6.7 ROS assay

ROS induction by flg22 was assayed and quantified as described [37]. Leaf discs (12 discs per genotype/treatment in each experiment) were pre-floated on water or 1 μM PSK overnight and total ROS accumulation was measured by chemiluminescence after adding 1 μM flg22. Alternatively, leaf discs were treated with PSK for shorter time (15 min - 5 h). To compare different experiments, ROS in WT + flg22 was set as 1. Relative ROS accumulation was quantified from at least 4 experiments for each PSK pretreatment.

6.8 Protein isolation and immunoblot analysis

11-day-old seedlings grown *in vitro* (3-5 seedlings per sample) or leaf discs (5-8 discs per sample) from soil-grown plants were treated with 1 μM or 200 nM PSK overnight and MAP kinases were activated by adding 1 μM or 200 nM flg22, respectively, for 7-15 min. Alternatively, plant samples were pretreated with PSK for shorter time (10-40 min). Total proteins were isolated by grinding tissue in cold isolation buffer (Tris HCl 150 mM pH 7.5, NaCl 150 mM, EDTA 5 mM, DTT 1 mM, protease inhibitor for plants (Sigma), phosphatase inhibitor (Pierce/Thermo Fisher) Triton X-100 1%). Proteins were resolved by SDS-PAGE, transferred to a PVDF membrane and probed with following rabbit antibodies: phospho-p44/42 MAPK (Erk1/2) (Thr202/Tyr204 (Cell Signaling Technologies, 1:1000-1:2000); MPK3 (Sigma, 1:2000); FLS2 (1:500) [67] and anti-rabbit-HRP secondary antibodies (Thermo Fisher). Proteins were detected by chemiluminescence using Bio-Rad ChemiDoc XRS+ imager. Relative band intensities were quantified from at least four experiments using Image Lab software (Bio-Rad) and normalized relative to total protein from Coomassie Blue-stained membranes, similar to a previously described method [37]. Different

treatment duration and peptide concertation gave similar results and the experiments were analyzed together by setting immunoblot signal in Col without PSK to 1.

6.9 Callose Deposition

Plants grown in 6-well cell culture dishes (5 seedlings per well) were treated with water or PSK solutions at day 7 for 24 hours, and then treated with water or flg22 solutions at day 8 for 24 hours. The treatments were conducted by adding PSK solution and flg22 solutions to the liquid 1/2 MS medium to achieve a final concentration of 100 nM and 1 μM respectively. The plants were fixed and stained with Aniline Blue as described in [68]. Callose deposits were quantified with Fiji using images taken with fluorescence microscope, utilizing 60 cotyledons from 30 seedlings per genotype and per treatment.

REFERENCES

1. Leyser, O. (2018). Auxin signaling. *Plant Physiology*, *176*(1), 465-479.

2. Davière, J. M., & Achard, P. (2013). Gibberellin signaling in plants. *Development*, *140*(6), 1147-1151.

3. Boller, T. (2005). Peptide signalling in plant development and self/non-self perception. *Current Opinion in Cell Biology*, *17*(2), 116-122.

4. Czyzewicz, N., Yue, K., Beeckman, T., & Smet, I. D. (2013). Message in a bottle: small signalling peptide outputs during growth and development. *Journal of Experimental Botany*, *64*(17), 5281-5296.

5. Matsubayashi, Y. (2014). Posttranslationally modified small-peptide signals in plants. *Annual Review of Plant Biology*, *65*, 385-413.

6. Matsubayashi, Y., & Sakagami, Y. (1996). Phytosulfokine, sulfated peptides that induce the proliferation of single mesophyll cells of Asparagus officinalis L. *Proceedings of the National Academy of Sciences*, *93*(15), 7623-7627.

7. Yang, H., Matsubayashi, Y., Nakamura, K., & Sakagami, Y. (2001). Diversity of Arabidopsis genes encoding precursors for phytosulfokine, a peptide growth factor. *Plant Physiology*, *127*(3), 842-851.

8. Lorbiecke, R., & Sauter, M. (2002). Comparative analysis of PSK peptide growth factor precursor homologs. *Plant Science*, *163*(2), 321-332.

9. Komori, R., Amano, Y., Ogawa-Ohnishi, M., & Matsubayashi, Y. (2009). Identification of tyrosylprotein sulfotransferase in Arabidopsis. *Proceedings of the National Academy of Sciences*, *106*(35), 15067-15072.

10. Kaufmann, C., & Sauter, M. (2019). Sulfated plant peptide hormones. *Journal of Experimental Botany*, *70*(16), 4267-4277.

11. Srivastava, R., Liu, J. X., & Howell, S. H. (2008). Proteolytic processing of a precursor protein for a growth-promoting peptide by a subtilisin serine protease in Arabidopsis. *The Plant Journal*, *56*(2), 219-227.

12. Stührwohldt, N., Dahlke, R. I., Steffens, B., Johnson, A., & Sauter, M. (2011). Phytosulfokine-α controls hypocotyl length and cell expansion in Arabidopsis thaliana through phytosulfokine receptor 1. *PLoS One*, *6*(6), e21054.

13. Hartmann, J., Fischer, C., Dietrich, P., & Sauter, M. (2014). Kinase activity and calmodulin binding are essential for growth signaling by the phytosulfokine receptor PSKR 1. *The Plant Journal*, *78*(2), 192-202.

14. Matsubayashi, Y., Ogawa, M., Morita, A., & Sakagami, Y. (2002). An LRR receptor kinase involved in perception of a peptide plant hormone, phytosulfokine. *Science*, *296*(5572), 1470-1472.

15. Hartmann, J., Stührwohldt, N., Dahlke, R. I., & Sauter, M. (2013). Phytosulfokine control of growth occurs in the epidermis, is likely to be non-cell autonomous and is dependent on brassinosteroids. *The Plant Journal*, *73*(4), 579-590.

16. Amano, Y., Tsubouchi, H., Shinohara, H., Ogawa, M., & Matsubayashi, Y. (2007). Tyrosine-sulfated glycopeptide involved in cellular proliferation and expansion in Arabidopsis. *Proceedings of the National Academy of Sciences*, *104*(46), 18333-18338.

17. Wang, J., Li, H., Han, Z., Zhang, H., Wang, T., Lin, G., ... & Chai, J. (2015). Allosteric receptor activation by the plant peptide hormone phytosulfokine. *Nature*, *525*(7568), 265-268.

18. Muleya, V., Wheeler, J. I., Ruzvidzo, O., Freihat, L., Manallack, D. T., Gehring, C., & Irving, H. R. (2014). Calcium is the switch in the moonlighting dual function of the ligand-activated receptor kinase phytosulfokine receptor 1. *Cell Communication and Signaling*, *12*, 1-5.

19. Irving, H. R., Cahill, D. M., & Gehring, C. (2018). Moonlighting proteins and their role in the control of signaling microenvironments, as exemplified by cGMP and phytosulfokine receptor 1 (PSKR1). *Frontiers in Plant Science*, *9*, 304270.

20. Sauter, M. (2015). Phytosulfokine peptide signalling. *Journal of Experimental Botany*, *66*(17), 5161-5169.

21. Matsubayashi, Y., Ogawa, M., Kihara, H., Niwa, M., & Sakagami, Y. (2006). Disruption and overexpression of Arabidopsis phytosulfokine receptor gene affects cellular longevity and potential for growth. *Plant Physiology*, *142*(1), 45-53.

22. Yu, L., Liu, Y., Liu, Y., Li, Q., Tang, G., & Luo, L. (2016). Overexpression of phytosulfokine-α induces male sterility and cell growth by regulating cell wall development in Arabidopsis. *Plant Cell Reports*, *35*, 2503-2512.

23. Mosher, S., Seybold, H., Rodriguez, P., Stahl, M., Davies, K. A., Dayaratne, S., ... & Kemmerling, B. (2013). The tyrosine-sulfated peptide receptors PSKR1 and PSY1R modify the immunity of Arabidopsis to biotrophic and necrotrophic pathogens in an antagonistic manner. *The Plant Journal*, *73*(3), 469-482.

24. Song, S., Morales Moreira, Z., Briggs, A. L., Zhang, X. C., Diener, A. C., & Haney, C. H. (2023). PSKR1 balances the plant growth–defence trade-off in the rhizosphere microbiome. *Nature Plants*, *9*(12), 2071-2084.

25. Field, B., & Osbourn, A. E. (2008). Metabolic diversification—independent assembly of operon-like gene clusters in different plants. *Science*, *320*(5875), 543-547.

26. Kaufmann, C., Stührwohldt, N., & Sauter, M. (2021). Tyrosylprotein sulfotransferase-dependent and-independent regulation of root development and signaling by PSK LRR receptor kinases in Arabidopsis. *Journal of Experimental Botany*, *72*(15), 5508-5521.

27. Rushton, P. J., Somssich, I. E., Ringler, P., & Shen, Q. J. (2010). WRKY transcription factors. *Trends in Plant Science*, *15*(5), 247-258.

28. Chen, F., Hu, Y., Vannozzi, A., Wu, K., Cai, H., Qin, Y., ... & Zhang, L. (2017). The WRKY transcription factor family in model plants and crops. *Critical Reviews in Plant Sciences*, *36*(5-6), 311-335.

29. Wani, S. H., Anand, S., Singh, B., Bohra, A., & Joshi, R. (2021). WRKY transcription factors and plant defense responses: latest discoveries and future prospects. *Plant Cell Reports*, *40*, 1071-1085.

30. Javed, T., & Gao, S. J. (2023). WRKY transcription factors in plant defense. *Trends in Genetics*.

31. Birkenbihl, R. P., Kracher, B., Roccaro, M., & Somssich, I. E. (2017). Induced genome-wide binding of three Arabidopsis WRKY transcription factors during early MAMP-triggered immunity. *The Plant Cell*, *29*(1), 20-38.

32. Tian, F., Yang, D. C., Meng, Y. Q., Jin, J., & Gao, G. (2020). PlantRegMap: charting functional regulatory maps in plants. *Nucleic Acids Research*, *48*(D1), D1104-D1113.

33. Evans, T. S., & Chen, B. (2022). Linking the network centrality measures closeness and degree. *Communications Physics*, *5*(1), 172.

34. Ogawa-Ohnishi, M., Yamashita, T., Kakita, M., Nakayama, T., Ohkubo, Y., Hayashi, Y., ... & Matsubayashi, Y. (2022). Peptide ligand-mediated trade-off between plant growth and stress response. *Science*, *378*(6616), 175-180.

35. Desrut, A., Moumen, B., Thibault, F., Le Hir, R., Coutos-Thévenot, P., & Vriet, C. (2020). Beneficial rhizobacteria Pseudomonas simiae WCS417 induce major transcriptional changes in plant sugar transport. *Journal of Experimental Botany*, *71*(22), 7301-7315.

36. Hu, Z., Zhang, H., & Shi, K. (2018). Plant peptides in plant defense responses. *Plant Signaling & Behavior*, *13*(8), e1475175.

37. Wu, S., Shan, L., & He, P. (2014). Microbial signature-triggered plant defense responses and early signaling mechanisms. *Plant Science*, *228*, 118-126.

38. Pieterse, C. M., Berendsen, R. L., de Jonge, R., Stringlis, I. A., Van Dijken, A. J., Van Pelt, J. A., ... & Bakker, P. A. (2021). Pseudomonas simiae WCS417: star track of a model beneficial rhizobacterium. *Plant and Soil*, *461*, 245-263.

39. Dröge-Laser, W., Snoek, B. L., Snel, B., & Weiste, C. (2018). The Arabidopsis bZIP transcription factor family—an update. *Current Opinion in Plant Biology*, *45*, 36-49.

40. Felix, G., Duran, J. D., Volko, S., & Boller, T. (1999). Plants have a sensitive perception system for the most conserved domain of bacterial flagellin. *The Plant Journal*, *18*(3), 265-276.

41. Denoux, C., Galletti, R., Mammarella, N., Gopalan, S., Werck, D., De Lorenzo, G., ... & Dewdney, J. (2008). Activation of defense response pathways by OGs and Flg22 elicitors in Arabidopsis seedlings. *Molecular Plant*, *1*(3), 423-445.

42. Tateda, C., Zhang, Z., Shrestha, J., Jelenska, J., Chinchilla, D., & Greenberg, J. T. (2014). Salicylic acid regulates Arabidopsis microbial pattern receptor kinase levels and signaling. *The Plant Cell*, *26*(10), 4171-4187.

43. Lassowskat, I., Böttcher, C., Eschen-Lippold, L., Scheel, D., & Lee, J. (2014). Sustained mitogen-activated protein kinase activation reprograms defense metabolism and phosphoprotein profile in Arabidopsis thaliana. *Frontiers in Plant Science*, *5*, 110384.

44. Wang, Y., Schuck, S., Wu, J., Yang, P., Döring, A. C., Zeier, J., & Tsuda, K. (2018). A MPK3/6-WRKY33-ALD1-pipecolic acid regulatory loop contributes to systemic acquired resistance. *The Plant Cell*, *30*(10), 2480-2494.

45. Wang, D., Wei, L., Liu, T., Ma, J., Huang, K., Guo, H., ... & Wang, Y. (2023). Suppression of ETI by PTI priming to balance plant growth and defense through an MPK3/MPK6-WRKYs-PP2Cs module. *Molecular Plant*, *16*(5), 903-918.

46. Hu, Z., Fang, H., Zhu, C., Gu, S., Ding, S., Yu, J., & Shi, K. (2023). Ubiquitylation of PHYTOSULFOKINE RECEPTOR 1 modulates the defense response in tomato. *Plant Physiology*, *192*(3), 2507-2522.

47. Salomon, S., & Robatzek, S. (2006). Induced endocytosis of the receptor kinase FLS2. *Plant Signaling & Behavior*, *1*(6), 293-295.

48. Spallek, T., Beck, M., Ben Khaled, S., Salomon, S., Bourdais, G., Schellmann, S., & Robatzek, S. (2013). ESCRT-I mediates FLS2 endosomal sorting and plant immunity. *PLoS Genetics*, *9*(12), e1004035.

49. Smith, J. M., Leslie, M. E., Robinson, S. J., Korasick, D. A., Zhang, T., Backues, S. K., ... & Heese, A. (2014). Loss of Arabidopsis thaliana Dynamin-Related Protein 2B reveals separation of innate immune signaling pathways. *PLoS Pathogens*, *10*(12), e1004578.

50. Luna, E., Pastor, V., Robert, J., Flors, V., Mauch-Mani, B., & Ton, J. (2011). Callose deposition: a multifaceted plant defense response. *Molecular Plant-Microbe Interactions*, *24*(2), 183-193.

51. Maekawa, S., Sato, T., Asada, Y., Yasuda, S., Yoshida, M., Chiba, Y., & Yamaguchi, J. (2012). The Arabidopsis ubiquitin ligases ATL31 and ATL6 control the defense response as well as the carbon/nitrogen response. *Plant Molecular Biology*, *79*, 217-227.

52. Kadota, Y., Shirasu, K., & Zipfel, C. (2015). Regulation of the NADPH oxidase RBOHD during plant immunity. *Plant and Cell Physiology*, *56*(8), 1472-1480.

53. Mbengue, M., Bourdais, G., Gervasi, F., Beck, M., Zhou, J., Spallek, T., ... & Robatzek, S. (2016). Clathrin-dependent endocytosis is required for immunity mediated by pattern recognition receptor kinases. *Proceedings of the National Academy of Sciences*, *113*(39), 11034-11039.

54. Ellinger, D., & Voigt, C. A. (2014). Callose biosynthesis in Arabidopsis with a focus on pathogen response: what we have learned within the last decade. *Annals of Botany*, *114*(6), 1349-1358.

55. Sanmartín, N., Pastor, V., Pastor-Fernández, J., Flors, V., Pozo, M. J., & Sánchez-Bel, P. (2020). Role and mechanisms of callose priming in mycorrhiza-induced resistance. *Journal of Experimental Botany*, *71*(9), 2769-2781.

56. Wang, Y., Li, X., Fan, B., Zhu, C., & Chen, Z. (2021). Regulation and function of defense-related callose deposition in plants. *International Journal of Molecular Sciences*, *22*(5), 2393.

57. Sheikh, A. H., Eschen-Lippold, L., Pecher, P., Hoehenwarter, W., Sinha, A. K., Scheel, D., & Lee, J. (2016). Regulation of WRKY46 transcription factor function by mitogen-activated protein kinases in Arabidopsis thaliana. *Frontiers in Plant Science*, *7*, 171759.

58. Sun, Y., Li, L., Macho, A. P., Han, Z., Hu, Z., Zipfel, C., ... & Chai, J. (2013). Structural basis for flg22-induced activation of the Arabidopsis FLS2-BAK1 immune complex. *Science*, *342*(6158), 624-628.

59. Ladwig, F., Dahlke, R. I., Stührwohldt, N., Hartmann, J., Harter, K., & Sauter, M. (2015). Phytosulfokine regulates growth in Arabidopsis through a response module at the plasma membrane that includes CYCLIC NUCLEOTIDE-GATED CHANNEL17, H^+-ATPase, and BAK1. *The Plant Cell*, *27*(6), 1718-1729.

60. Lamesch, P., Berardini, T. Z., Li, D., Swarbreck, D., Wilks, C., Sasidharan, R., ... & Huala, E. (2012). The Arabidopsis Information Resource (TAIR): improved gene annotation and new tools. *Nucleic Acids Research*, *40*(D1), D1202-D1210.

61. Kim, D., Paggi, J. M., Park, C., Bennett, C., & Salzberg, S. L. (2019). Graph-based genome alignment and genotyping with HISAT2 and HISAT-genotype. *Nature Biotechnology*, *37*(8), 907-915.

62. Mortazavi, A., Williams, B. A., McCue, K., Schaeffer, L., & Wold, B. (2008). Mapping and quantifying mammalian transcriptomes by RNA-Seq. *Nature Methods*, *5*(7), 621-628.

63. Love, M. I., Huber, W., & Anders, S. (2014). Moderated estimation of fold change and dispersion for RNA-seq data with DESeq2. *Genome Biology*, *15*, 1-21.

64. Huang, D. W., Sherman, B. T., & Lempicki, R. A. (2009). Systematic and integrative analysis of large gene lists using DAVID bioinformatics resources. *Nature Protocols*, *4*(1), 44-57.

65. Gu, Z., Eils, R., & Schlesner, M. (2016). Complex heatmaps reveal patterns and correlations in multidimensional genomic data. *Bioinformatics*, *32*(18), 2847-2849.

66. Oliveros, J. C. (2007). VENNY. An interactive tool for comparing lists with Venn Diagrams. *http://bioinfogp.cnb.csic.es/tools/venny/index.html*.

67. Chinchilla, D., Zipfel, C., Robatzek, S., Kemmerling, B., Nürnberger, T., Jones, J. D., ... & Boller, T. (2007). A flagellin-induced complex of the receptor FLS2 and BAK1 initiates plant defence. *Nature*, *448*(7152), 497-500.

68. Mason, K. N., Ekanayake, G., & Heese, A. (2020). Staining and automated image quantification of callose in Arabidopsis cotyledons and leaves. In *Methods in Cell Biology* (Vol. 160, pp. 181-199). Academic Press.